

A POSTERIORI TRANSIT PROBABILITIES

DANIEL J. STEVENS AND B. SCOTT GAUDI

Department of Astronomy, The Ohio State University, 140 W. 18th Ave., Columbus, OH, USA 43210

Draft version May 8, 2013

ABSTRACT

Given the radial velocity (RV) detection of an unseen companion, it is often of interest to estimate the probability that the companion also transits the primary star. Typically, one assumes a uniform distribution for the cosine of the inclination angle i of the companion's orbit. This yields the familiar estimate for the *prior* transit probability of $\sim R_*/a$, given the primary radius R_* and orbital semimajor axis a , and assuming small companions and a circular orbit. However, the *posterior* transit probability depends not only on the prior probability distribution of i but also on the prior probability distribution of the companion mass M_c , given a measurement of the product of the two (the minimum mass $M_c \sin i$) from an RV signal. In general, the posterior can be larger or smaller than the prior transit probability. We derive analytic expressions for the posterior transit probability assuming a power-law form for the distribution of true masses, $d\Gamma/dM_c \propto M_c^\alpha$, for integer values $-3 \leq \alpha \leq 3$. We show that for low transit probabilities, these probabilities reduce to a constant multiplicative factor f_α of the corresponding prior transit probability, where f_α in general depends on α and an assumed upper limit on the true mass. The prior and posterior probabilities are equal for $\alpha = -1$. The posterior transit probability is ~ 1.5 times larger than the prior for $\alpha = -3$ and is $\sim 4/\pi$ times larger for $\alpha = -2$, but is less than the prior for $\alpha \geq 0$, and can be arbitrarily small for $\alpha > 1$. We also calculate the posterior transit probability in different mass regimes for two physically-motivated mass distributions of companions around Sun-like stars. We find that for Jupiter-mass planets, the posterior transit probability is roughly equal to the prior probability, whereas the posterior is likely higher for Super-Earths and Neptunes ($10M_\oplus - 30M_\oplus$) and Super-Jupiters ($3M_{\text{Jup}} - 10M_{\text{Jup}}$), owing to the predicted steep rise in the mass function toward smaller masses in these regimes. We therefore suggest that companions with minimum masses in these regimes might be better-than-expected targets for transit follow-up, and we identify promising targets from RV-detected planets in the literature. Finally, we consider the uncertainty in the transit probability arising from uncertainties in the input parameters, and the effect of ignoring the dependence of the transit probability on the true semimajor axis on i .

1. INTRODUCTION

Transiting planets have become the primary resource for characterizing the detailed properties of exoplanets. When complemented by RV measurements of the planet's orbital eccentricity, period, argument of periastron, and velocity semiamplitude, as well as by measurements of the stellar host's mass and radius, a photometric transit allows for the measurement of the mass, radius, density, and surface gravity of the planet. With these basic parameters in hand, a transiting planet system is then amenable to a profusion of follow-up observations, which can then yield an impressive array of physical properties of the planet and star (see Winn 2011 for a review).

Transiting planets are currently discovered via two different methods. First, planets that are initially discovered by RV measurements are monitored photometrically during the predicted time of inferior conjunction, in order to detect the small fraction that transit. In fact, the first identified transiting planet HD 209458b was discovered in this manner (Charbonneau et al. 2000; Henry et al. 2000). Second, photometric transit surveys synoptically monitor large numbers of stars to search for eclipse signals consistent with planetary-sized companions. These candidate transiting planets are then subjected to a battery of follow-up observations in order to eliminate false positives and ultimately confirm the planet by measuring its RV signal and, in doing so, its mass.

Because it is relatively easy and inexpensive to moni-

tor large numbers of stars photometrically with the precision needed to detect planetary transit signals, photometric surveys for transiting planets can readily overcome the intrinsic rarity of transiting systems and efficiently identify large samples of candidates. Indeed, the vast majority of confirmed transiting planets were discovered in dedicated ground-based transit surveys (e.g., Udalski et al. 2002; Konacki et al. 2003; Alonso et al. 2004; McCullough et al. 2006; Bakos et al. 2007; Collier Cameron et al. 2007; Weldrake et al. 2008; Alsubai et al. 2011; Siverd et al. 2012). In addition, Kepler has discovered over 2,700 transiting planet candidates (Batalha et al. 2013; Burke et al. 2013) — an amount greater than that of all previously-known exoplanets, although most of these lack precision RV confirmation and so lack precision mass estimates. However, the cadence, photometric precision, and total number of observations needed to achieve robust detections of transit signals typically requires monitoring relatively small fractions of the sky at a time; as a result, photometric transit surveys typically identify transiting planets orbiting relatively faint ($V \gtrsim 10$) stars.

On the other hand, because of the relatively demanding observational requirements for precision RV measurements — in particular, high-resolution spectra, broad wavelength coverage, and a high signal-to-noise ratio — RV surveys must, in general, target bright stars in series with relatively large aperture telescopes. Because

of these constraints, only a few thousands of stars have been monitored with precision RV. When combined with the rarity of planetary companions in general and transiting planets in particular, only eight of the planets originally detected via RV have been subsequently shown to transit (Barbieri et al. 2007; Winn et al. 2011a; Demory et al. 2011; Charbonneau et al. 2000; Henry et al. 2000; Sato et al. 2005; Bonfils et al. 2012; Bouchy et al. 2005; Moutou et al. 2009; Fossey et al. 2009; Gillon et al. 2007). Nevertheless, because they all orbit bright stars, these systems are the most amenable to follow-up programs and so are extraordinarily valuable. Indeed, these systems are some of best-characterized planets outside our own solar system.

Fortunately, it is likely that the both the sample size and diversity of transiting planets originally discovered by precise RV surveys will expand considerably in the future via several avenues. Amongst the currently-known RV planets, it is expected that there exist a handful of long-period transiting planets that have not yet been photometrically identified. The Transit Ephemerides Refinement and Monitoring Survey (Kane et al. 2010a) aims to identify these systems by first refining the orbits (and the estimated time of conjunction) of the most promising systems (i.e. those with the highest transit probabilities) and then following these up photometrically (Seagroves et al. 2003). Even more promising, samples of RV-detected planets have been and will continue growing significantly. The measurement precision of optical RV surveys has steadily improved, allowing for the detection of first Neptune-mass (McArthur et al. 2004; Butler et al. 2004; Lovis et al. 2006), then Super-Earth mass (Rivera et al. 2005; Udry et al. 2007; Mayor et al. 2009), and most recently Earth-mass (Dumusque et al. 2012) companions, all of which are intrinsically more numerous than gas giant planets (Howard et al. 2010; Mayor et al. 2011). In the near future, the development of dedicated near-IR precision RV instruments (e.g., Bean et al. 2010; Plavchan et al. 2013; Rayner & PRVS Team 2007; Mahadevan et al. 2012) will enable surveys of large, previously-inaccessible samples of low-mass stars, and will also have enhanced sensitivity to low-mass companions. Finally, massive parallel RV surveys, such as the Multi-object APO Radial Velocity Exoplanet Large-area Survey (MARVELS) (Ge et al. 2008; Eisenstein et al. 2011), may allow for surveys of giant planets orbiting somewhat fainter but considerably more numerous stars.

It is likely that substantial photometric follow-up resources will be necessary to identify the transiting systems from these anticipated large samples of RV-detected exoplanets. For example, the CHaracterizing ExoPlanets Satellite (CHEOPS), planned for launch in 2017, is a satellite dedicated just to this purpose (Feldt et al. 2007). It is important that these necessarily-limited photometric follow-up resources be allocated optimally to maximize the yield of transiting planets.

The most important input to optimizing follow-up efforts is an estimate of the transit probability P_{tr} . The transit probability is defined as the probability, given both the properties of the companion that are inferred from RV measurements and the properties of the host star that are inferred from auxilliary measurements, that the orbit of the companion is inclined such that it passes in front of the host star from our perspective at some

point during its orbit. The simplest and most commonly used estimate of the transit probability is (Borucki & Summers 1984; Sackett 1999),

$$P_{tr} = \frac{R_*}{a}, \quad (1)$$

where R_* is the radius of the host star and a is the semi-major axis of the companion’s orbit. This estimate makes a number of assumptions that are widely appreciated, including: a circular orbit for the companion, a companion radius R_c that is much smaller than the stellar radius, and a uniform distribution for the cosine of the inclination angle i of the orbit. The effect of the finite size of the planetary companion can be easily included by, e.g., replacing $R_* \rightarrow R_* + R_c$ for grazing transits. The effect of eccentric orbits on the transit probability has been explored in a number of papers (Seagroves et al. 2003; Barnes 2007; Burke 2008; Kane & von Braun 2008). Eccentricity can boost the transit probability relative to the naive estimate in Equation 1, particularly for some favorable geometries. HD 17156 b, with its eccentricity of 0.67 (Fischer et al. 2007; Barbieri et al. 2007), and HD 80606 b, with an eccentricity of 0.927 (Naef et al. 2001; Moutou et al. 2009; Fossey et al. 2009), are dramatic examples of these effects. Beatty & Seager (2010) found that a prior constraint on the inclination of the host star can also boost the transit probability (see also Sackett 1999; Watson et al. 2010), assuming the axis of the companion orbit is aligned with the spin axis of the star. Finally, Kane & von Braun (2008) showed that constraints on secondary eclipses can also affect the transit probability.

However, there are some additional assumptions inherent in Equation 1 that are less widely appreciated and that can also affect the transit probability; we explore several of these here. In particular, the *posterior* probability distribution of the orbit inclination angle i , given the detection of an RV companion, depends not only on the prior distribution of i but also on the prior distribution of the true mass of the companion M_c . While the prior distribution of i is well-known (and is simply uniform in $\cos i$), the prior distribution of M_c is generally not well-constrained — at least, not in the regimes of interest for exoplanet surveys. Although the effect of the prior distribution of M_c on the transit probability has been noted and estimated previously for a few specific cases (e.g., Wisniewski et al. 2012), to the best of our knowledge it has not been explored in any detail. Previous authors have noted the dependence of the posterior probability distribution of i (and thus M_c) on the prior distributions of i and M_c (e.g., Ho & Turner 2011; Lopez & Jenkins 2012). The fact that the transit probability also depends on both these priors follows trivially from this result. In addition, here we explore two additional effects that we also believe have not previously been discussed in detail. First, we estimate the effects of uncertainties on the RV observables and host star properties on the estimated transit probability. Second, we note that the semimajor axis in Equation 1 is properly the true semimajor axis (rather than the minimum semimajor axis), which is not known from RV measurements alone, and indeed depends on the orbital inclination for a given set of observables.

The plan for this paper is as follows. In Section 2, we

review the observables for RV detected companions, and reiterate how these can be used to derive the familiar *a priori* transit probability from RV data. In Section 3, we derive the *a posteriori* transit probability for an observed minimum mass M_0 and true mass distribution dN/dM_c . In Section 4, we explore the posterior transit probability for power-law mass distributions, discuss issues of convergence for certain power-law distributions, and show that the posterior transit probability can be expressed as a simply scaling of the prior probability for low transit probabilities. We calculate posterior transit probabilities for different regimes of two model companion mass distributions in Section 5. In Section 6, we compare the number of known transiting RV-discovered transiting planets with the number expected based on the naive prior transit probability. We also compare the posterior and prior transit probabilities for known RV planets, and identify planets whose posterior transit probabilities are both high and substantially higher than the corresponding naive prior probabilities. In Section 7, we discuss the effect of propagating parameter uncertainties on the estimate of the transit probability, as well as the effect of assuming the minimum semimajor axis to estimate the transit probability. We summarize our results in Section 8.

2. PROBLEM SET-UP

Consider the RV detection of a faint companion, such as a single-lined spectroscopic binary. A well-sampled, high signal-to-noise ratio RV detection yields estimates of the orbital period T , semi-amplitude K , eccentricity e , the argument of periastron of the host star ω , and the time at some reference point in the orbit (e.g. the periastron). The semi-amplitude K is related to T , e , the host star mass M_* , the companion mass M_c , and the orbital inclination i via

$$K = \left(\frac{2\pi G}{T} \right)^{1/3} \frac{M_c \sin i}{(M_* + M_c)^{2/3}} (1 - e^2)^{-1/2}. \quad (2)$$

As is well known, the only model-independent physical quantity one can infer about a single-lined spectroscopic binary purely from direct observables is the mass function \mathcal{M} , which is defined as

$$\mathcal{M} \equiv \frac{(M_c \sin i)^3}{(M_* + M_c)^2} = \frac{K^3 T}{2\pi G} (1 - e^2)^{3/2}. \quad (3)$$

Generally, one can also estimate the mass (and radius R_*) of the host star through a variety of methods. With an estimate of M_* one can use the measured value of \mathcal{M} to determine M_c as a function of i by solving the resulting cubic equation for M_c . One can then also estimate the semimajor axis of the orbit as a function of i ,

$$a = \left(\frac{G[M_* + M_c(i)]}{4\pi^2} \right)^{1/3} T^{2/3} \quad (4)$$

If one has independent reason to believe that $M_c \ll M_*$, then the “minimum mass” of the companion can be

estimated directly by,

$$\begin{aligned} M_0 &\equiv M_c \sin i \\ &= K \left(\frac{T}{2\pi G} \right)^{1/3} (1 - e^2)^{1/2} (M_* + M_c)^{2/3} \\ &\simeq K \left(\frac{T}{2\pi G} \right)^{1/3} (1 - e^2)^{1/2} M_*^{2/3}. \end{aligned} \quad (5)$$

An excellent approximation for the condition that the companion transits the host is that its projected separation from the center of the host star at the time of inferior conjunction is less than or equal to the sum of R_* and the radius of the companion R_c (Kipping 2008; Winn 2011). The orbital separation of the companion from the host at the time of inferior conjunction is

$$r_c = \frac{a(1 - e^2)}{1 + e \sin \omega}, \quad (6)$$

leading to the condition for a transit,

$$r_c \cos i \leq R_* + R_c. \quad (7)$$

Or, in terms of a limit on the inclination,

$$\cos i \leq \left(\frac{R_* + R_c}{a} \right) \left(\frac{1 + e \sin \omega}{1 - e^2} \right). \quad (8)$$

It is straightforward to demonstrate that, for isotropically-distributed orbit normals, the probability density distribution of $\cos i$ is uniform. In the absence of any information, we expect the orbits of binary systems to be isotropic, i.e. to have no preference for a given orientation. Therefore, the *a priori* probability density distribution of $\cos i$ is expected to be uniform, and the *a priori* transit probability is given by

$$P_{tr,0} = \left(\frac{R_* + R_c}{a} \right) \left(\frac{1 + e \sin \omega}{1 - e^2} \right). \quad (9)$$

In the case of a circular orbit and $R_c \ll R_*$, we recover the familiar transit probability $P_{tr,0} = R_*/a$.

However, once one makes a measurement of the companion’s minimum mass¹ M_0 — i.e. the product of M_c and $\sin i$ — the transit probability then depends not only on the prior probability density distribution of i but also on the prior probability density distribution of M_c . That the transit probability depends on the prior on M_c can be seen intuitively using the following example: Assume that one had prior knowledge that objects of mass $< M_{min}$ did not exist. Then, if one detected a companion with minimum mass $M_0 = 0.1 M_{min}$, one would be certain that the true mass M_c was at least ten times larger than the minimum mass, and therefore that $\sin i < 0.1$, or $\cos i > 0.995$. Provided that the prior transit probability $P_{tr,0} < 0.995$, the true *a posteriori* transit probability would be zero, since one would be certain that object did not transit.

We derive the general expression for the *a posteriori* transit probability in the next section. Before moving on, however, we note one subtlety that we ignored in the previous discussion. The semimajor axis a in equation 9 is the true semimajor axis, which depends on M_c and

¹ More precisely, once makes a measurement of the mass function.

thus on i . Therefore, in order to estimate the transit probability, one must either solve simultaneously for a and the critical inclination for a transit, or use an approximation to a . We return to this point in Section 7.2.

3. A POSTERIORI TRANSIT PROBABILITY

Bayes' Theorem gives the conditional probability density of event A given event B as

$$P(A|B) = \frac{P(B|A)P(A)}{P(B)}. \quad (10)$$

For our case, $A = \cos i$ and $B = M_0$. Then the probability density of $\cos i$ given a measurement of M_0 is

$$P(\cos i|M_0) = \frac{P(M_0|\cos i)P(\cos i)}{P(M_0)}, \quad (11)$$

where $P(M_0) = \int P(M_0|\cos i)P(\cos i)d\cos i$ and the integral is over the allowed range of $\cos i$. If we consider some maximum true mass $M_{c,max}$, then the integral is evaluated from $\cos i = 0$ to some minimum inclination angle i_{min} such that $\cos i_{min} = \sqrt{1 - (\sin i_{min})^2} = [1 - (M_0/M_{c,max})^2]^{1/2}$.

The prior probability density of $\cos i$ is uniform; we write this as

$$\frac{d\Gamma}{d\cos i} = P(\cos i) = \text{const.} \quad (12)$$

Here, Γ defines the rate or distribution, so $d\Gamma/d\cos i$ is the prior probability density with respect to $\cos i$. The probability density of M_0 given $\cos i$, $P(M_0|\cos i)$, is just the prior probability density of M_p times the Jacobian between M_c and M_0 , i.e.

$$P(M_0|\cos i) = \frac{d\Gamma}{dM_c} \frac{dM_c}{dM_0} = \frac{d\Gamma}{dM_c} \frac{1}{\sin i}, \quad (13)$$

where $d\Gamma/dM_c = P(M_c)$ is the prior probability density of the true mass M_c . Thus,

$$P(\cos i|M_0) = \frac{\frac{d\Gamma}{dM_c} \frac{1}{\sin i}}{\int_0^{\cos i_{min}} \frac{d\Gamma}{dM_c} \frac{1}{\sin i} d\cos i}. \quad (14)$$

Finally, the probability that the companion transits is the (cumulative) probability that $\cos i$ is less than the critical value for a transit, which is

$$P_{tr}(\cos i \leq X) = \frac{\int_0^X \frac{d\Gamma}{dM_c} \frac{1}{\sin i} d\cos i}{\int_0^{\cos i_{min}} \frac{d\Gamma}{dM_c} \frac{1}{\sin i} d\cos i}. \quad (15)$$

Here, we have defined the ratio of sum of the radii to r_c , i.e., the prior transit probability, as

$$X \equiv \frac{R_* + R_c}{r_c} = \left(\frac{R_* + R_c}{a} \right) \left(\frac{1 + e \sin \omega}{1 - e^2} \right), \quad (16)$$

4. POSTERIOR TRANSIT PROBABILITIES FOR POWER-LAW MASS DISTRIBUTIONS

4.1. Functional Forms

Assume that $d\Gamma/dM_c = CM_c^\alpha$, where C is a normalization constant. Then $d\Gamma/dM_c = C \left(\frac{M_0}{\sin i} \right)^\alpha =$

$CM_0^\alpha (1 - \cos^2 i)^{-\alpha/2}$ and Equation (15) becomes

$$P_{tr} = \frac{\int_0^X (1 - \cos^2 i)^{-\frac{(\alpha+1)}{2}} d\cos i}{\int_0^{\cos i_{min}} (1 - \cos^2 i)^{-\frac{(\alpha+1)}{2}} d\cos i}. \quad (17)$$

It is clear from this expression that, for $\alpha = -1$ (a uniform distribution in $\log M_c$), the posterior transit probability is equal to the prior transit probability. The integrand in the denominator is evaluated up to $\cos i_{min}$ to allow for an upper mass limit on the prior distribution of M_c . This is strictly necessary for $\alpha \geq 1$ because this integral diverges. For $\alpha < 1$, the integral converges, and so for simplicity we will take $\cos i_{min} = 1$ for these cases. We discuss the effect of the choice of i_{min} (or $M_{c,max}$) on the transit probability for $\alpha \geq 1$ in Section 4.2.

Since X and $\cos i_{min}$ are never greater than one, we can re-write Equation (17) as

$$P_{tr} = \frac{X [{}_2F_1(\frac{1}{2}, \frac{\alpha+1}{2}; \frac{3}{2}; X^2)]}{{}_2F_1(\frac{1}{2}, \frac{\alpha+1}{2}; \frac{3}{2}; \cos^2 i_{min})}, \quad (18)$$

where ${}_2F_1(a, b; c; d)$ is the Gaussian (or ordinary) hypergeometric function:

$${}_2F_1(a, b; c; d) = \sum_{k=0}^{\infty} \frac{(a)_k (b)_k d^k}{(c)_k k!}, \quad (19)$$

where $(x)_n$ is the Pochhammer symbol or rising factorial,

$$(x)_k = \begin{cases} 1 & \text{if } k = 0 \\ \prod_{j=0}^{k-1} x + j & \text{if } k > 0 \end{cases}. \quad (20)$$

The transit probability in equation 17 can be written using analytic functions for specific values of α . Table 1 gives these functions for integer values of α between -3 and 3, and the solid lines in the top panel of Figure 1 shows P_{tr} versus X for these α values. Our posterior distributions for $\cos i$ agree with the M_c posteriors given M_0 of Ho & Turner (2011) save for $\alpha = 1$; using their notation for the numerator of the companion-mass posterior, $\Phi(M_0, X, \alpha)$, we find that $\Phi(M_0, X, 1) = \log(\sqrt{X^2 - 1} + X)$ instead of $\Phi(M_0, X, 1) = \log(2\sqrt{X^2 - 1} + X)$ (cf. Equation 19 of Ho & Turner 2011).

Note that when x is a negative integer, $(x)_k$ is zero if $k \geq -x + 1$. The hypergeometric function in Eq. 19 thus has $-b + 1$ terms when b is a negative integer. Therefore, when α is an odd negative integer (i.e. $\alpha = -1, -3, -5, \dots$), the transit probability can be written as an odd polynomial in X of order $|\alpha|$ with $(-\alpha + 1)/2$ terms. For $\alpha = -1$, the hypergeometric functions in the numerator and denominator of Equation 18 are unity, and thus the transit probability is simply X — i.e. the prior transit probability.

Smaller α corresponds to a prior increasingly weighted toward smaller values of M_c . For a given M_0 , $M_c = M_0/\sin i \propto 1/\sin i$, so larger $\sin i$ values are increasingly preferred for smaller α . As a result, smaller $\cos i$ values are more likely, and the transit probability is higher, as illustrated in Figure 1.

We can also express Equation (17) as a function of period with Equation (4). We assume that $M_* = M_\odot$, $R_* = R_\odot$, and $R_c \ll R_*$. The top panel of Figure 2 shows

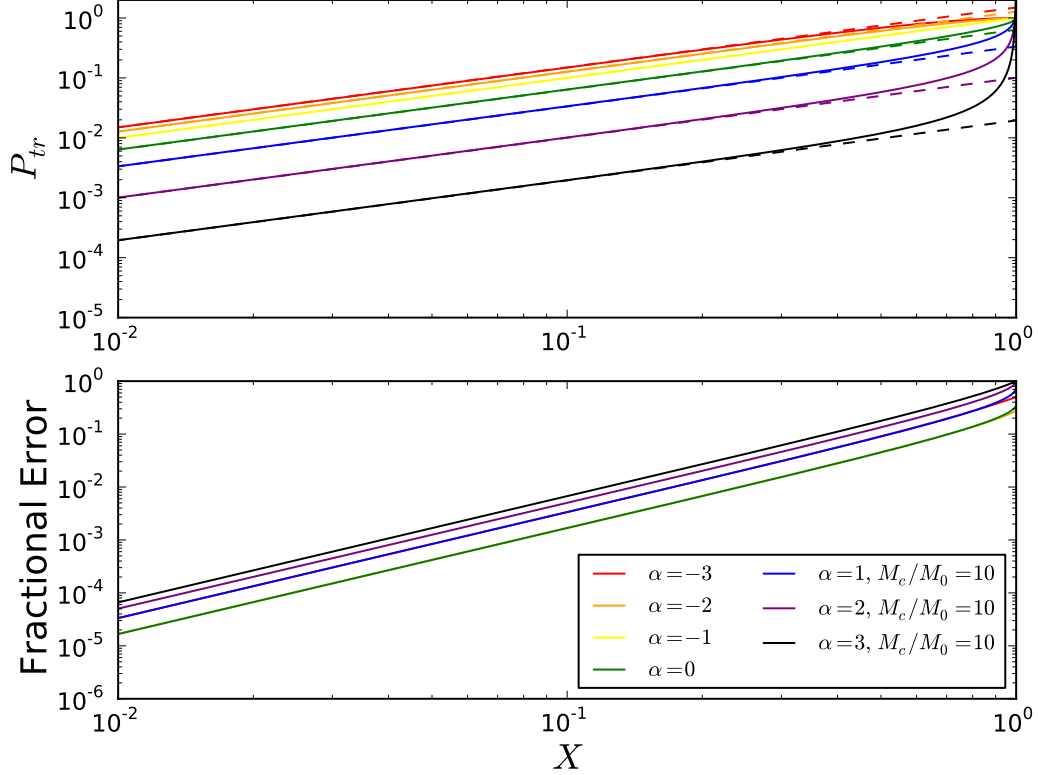


Figure 1. Posterior transit probability distributions as a function of the prior transit probability X for power-law true mass distributions with indices $\alpha = -3, -2, -1, 0, 1, 2$, and 3 . For $\alpha \geq 1$, we set $M_{c,max}/M_0 = 10$ or $\sin i_{min} = 0.1$ since the denominator of Equation (17) does not converge for these values of α . For $\alpha = -1$, the posterior is the same as the prior distribution, so $P_{tr} = X$. The solid lines show the exact posterior, while the dashed lines show the first-order Taylor series expansion centered at $X = 0$. For small X , the posterior transit probability is approximately a constant multiple of the prior probability. The bottom panel shows the fractional deviation between the full and approximate probabilities.

the posterior transit probabilities for the same power-law true mass distributions as a function of period. The dependence on the power-law true mass distribution can create a factor of $\sim 10^2$ difference in the posterior transit probability at a given period for power-law exponents in the range $\alpha = -3$ to 3 . This disparity decreases for very small orbital periods since $P_{tr} \rightarrow 1$ as $T \rightarrow 0$.

4.2. Dependence on Maximum M_c for $\alpha \geq 1$

As noted previously, the denominator of Equation (17) does not converge for $\cos i_{min} = 1$ when $\alpha \geq 1$. In Figure 3 we show the sensitivity of the posterior transit probability to $\cos i_{min}$ for $\alpha = 1, 2$, and 3 . We normalized P_{tr} to its value assuming $M_{c,max}/M_0 = 1$ ($\sin i_{min} = 10$). Since $M_c/M_0 = \frac{1}{\sin i} = (1 - \cos^2 i)^{-1/2}$, increasing $M_{c,max}$ corresponds to increasing $\cos i_{min}$, and therefore lowering the transit probability. For $\alpha = 1$, P_{tr} diverges logarithmically, and therefore the precise choice of $M_{c,max}$ does not strongly affect the implied transit probability, for reasonable values.

On the other hand, P_{tr} diverges more strongly for $\alpha > 1$, and in particular depends sensitively on $M_{c,max}$, and can be arbitrarily small. Accurate estimates of the transit probability of companions with minimum masses in such steeply-rising portions of the companion mass function therefore require reasonably narrow constraints

on $M_{c,max}$. In some cases, other evidence can be used to place a limit on $M_{c,max}$. For example, companions around very massive main-sequence stars can often be ruled out based on the lack of evidence of flux from the companion or a second set of spectral lines (e.g., Fleming et al. 2012).

4.3. Taylor Approximations

The simple linear behavior for small values of X exhibited in Figures 1 and 2 invites us to make a first-order Taylor approximation for P_{tr} centered at $X = 0$. The numerator of Equation (18) can be written as

$$X \left[{}_2F_1 \left(\frac{1}{2}, \frac{\alpha+1}{2}; \frac{3}{2}; X^2 \right) \right] = X \left[\sum_{k=0}^{\infty} \frac{\left(\frac{-[\alpha+1]}{2} \right)_k}{1+2k} \frac{X^{2k}}{k!} \right] = X[1 + \mathcal{O}(X^2)]. \quad (21)$$

This allows us to express the Taylor approximation as

$$P_{tr} = f_{\alpha} X + \mathcal{O}(X^3). \quad (22)$$

In other words, the posterior transit probability for power-law priors on the companion mass is equal to the prior transit probability times a constant scale factor f_{α} , up to third order in X . The scale factor f_{α} depends only on α and i_{min} , and is simply equal to the inverse

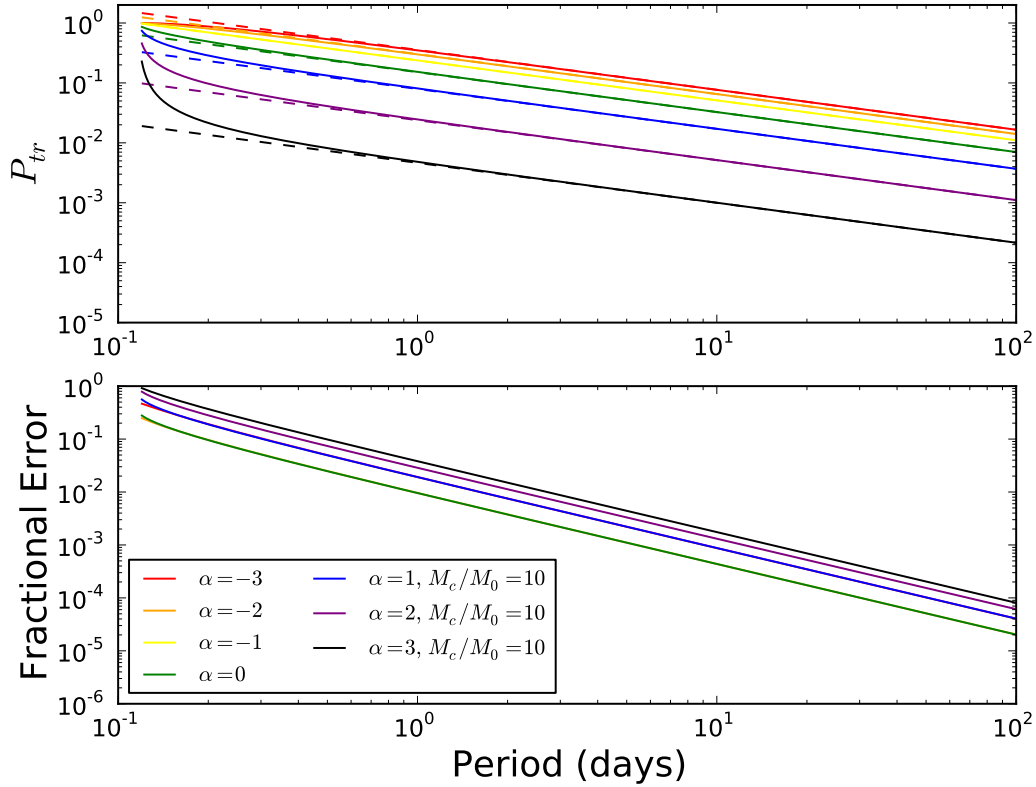


Figure 2. The top panel shows the posterior transit probability distributions as a function of period (solid lines) and their corresponding first-order Taylor approximations (dashed lines) for integer values of α between -3 and 3. We assume a solar mass and radius. For a given period, the top panel indicates that the posterior transit probability can differ by nearly a factor of 10^2 for different α . The difference in transit probabilities for exceptionally short periods decreases rapidly with decreasing period, converging to 1 for $T \rightarrow 0$. The bottom panel shows the fractional deviation of the first-order Taylor approximations to the full analytical transit probabilities.

of the denominator in the full expression for the transit probability,

$$f_\alpha \equiv \left[{}_2F_1 \left(\frac{1}{2}, \frac{\alpha+1}{2}; \frac{3}{2}; \cos^2 i_{\min} \right) \right]^{-1}. \quad (23)$$

For $\alpha < 1$, we can use Gauss' Theorem to express f_α in terms of Gamma functions,

$$f_\alpha = \frac{2\Gamma(1 - \frac{\alpha}{2})}{\sqrt{\pi} \Gamma(\frac{1-\alpha}{2})}. \quad (24)$$

It can be shown that this expression diverges for $\alpha \geq 1$. Furthermore, for $\alpha \ll -1$, we can use Stirling's approximation that $n! \approx \sqrt{2\pi n} n^n e^{-n}$ and the identity $n! = \Gamma(n+1)$ to approximate equation (24) as

$$f_\alpha \simeq \sqrt{\frac{-2\alpha}{\pi e}} \left(1 + \frac{1}{\alpha} \right)^{\alpha/2}. \quad (25)$$

An alternate expression for f_α in this regime that is somewhat less accurate, but also somewhat simpler is,

$$f_\alpha \sim \sqrt{\frac{-2\alpha}{\pi}}. \quad (26)$$

This can be derived from either Equation 25 or directly from the definition of f_α in equation 23, by using the

definition of the exponential function, $e^x \equiv \lim_{n \rightarrow \infty} (1 + x/n)^n$.

Figure 4 shows the exact value of f_α for $\alpha \leq 0$, as well as the two approximations given in Equations 25 and 26. We find that Equation 25 is an excellent approximation to f_α , deviating by $< 10\%$ for $\alpha \leq -1.7$ and by $< 1\%$ for $\alpha \leq -4.4$. Equation 26 is a somewhat poorer, but still accurate, approximation, deviating by $\lesssim 10\%$ for $\alpha \leq -2.5$. Interestingly, the boost factor does not converge for $\alpha \rightarrow -\infty$, and thus the posterior transit probability can be arbitrarily large even for small prior transit probabilities, if one allows for a mass function that rises arbitrarily steeply toward small masses. This implies that detected RV companions with minimum masses near a large jump in the mass function toward lower masses will have quite high transit probabilities.

The exact scale factors for several values of α are given in Table 1. We find the transit probability is boosted by $\sim 30\%$ for $\alpha = -2$, and by 50% for $\alpha = -3$.² However, the transit probability is reduced by $\sim 64\%$ for $\alpha = 0$ ($f_0 = 2/\pi$), and by larger amounts for $\alpha > 0$.

The linear approximations to P_{tr} are plotted as dashed lines in the top panels of Figures 1 and 2, and the bottom

² We note that $f_{-5} = 15/8 \sim 1.9$, $f_{-7} = 35/16 \sim 2.2$, $f_{-9} = 315/128 \sim 2.5$.

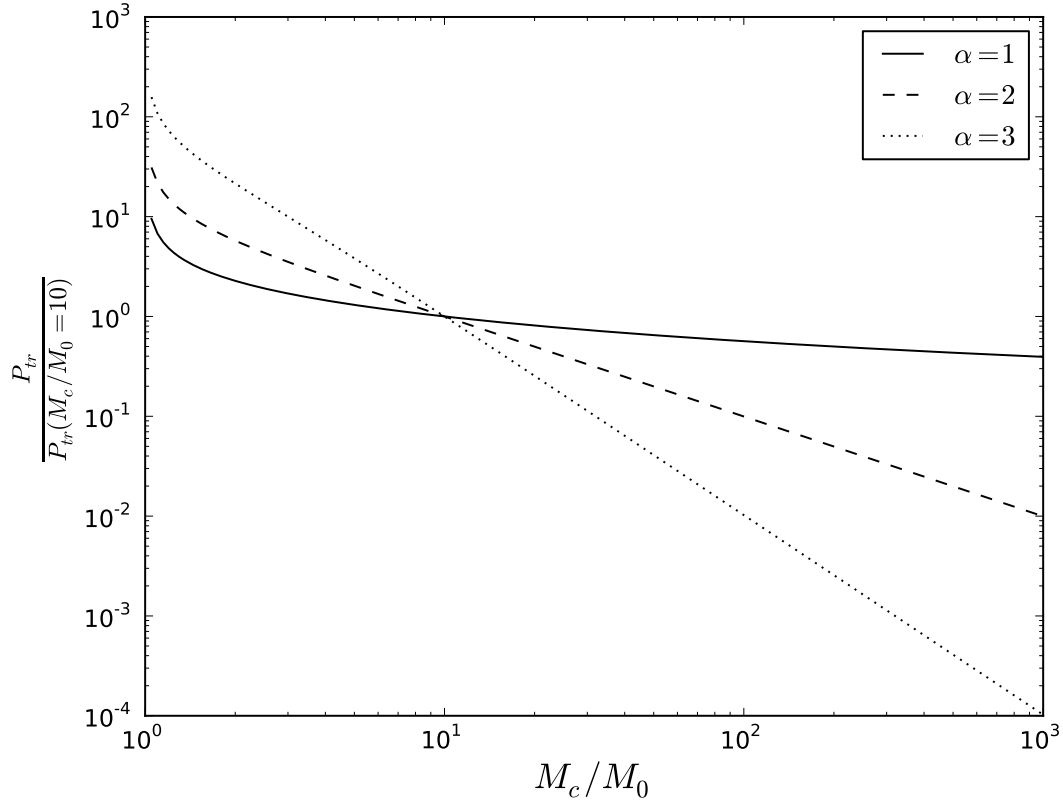


Figure 3. Posterior transit probabilities for $\alpha = 1, 2$, and 3 as a function of M_c/M_0 , normalized to the corresponding transit probability with $M_c/M_0 = 10$. Increasing M_c/M_0 corresponds to increasing $\cos i_{min}$. P_{tr} diverges only logarithmically for $\cos i_{min}$ approaching unity for $\alpha = 1$, but diverges more rapidly for $\alpha > 1$, as illustrated for the specific cases $\alpha = 2$ and 3 .

Table 1
Posterior Transit Probabilities and Scale Factors

Power-law Index α	$P_{tr}(X)$	f_α	Max X for % Error		
			$\leq 1\%$	$\leq 5\%$	$\leq 10\%$
-3	$\frac{3}{2}(X - \frac{X^3}{3})$	$3/2$	0.17	0.38	0.52
-2	$\frac{2}{\pi}(X\sqrt{1-X^2} + \arcsin X)$	$4/\pi$	0.24	0.52	0.71
-1	X	1	—	—	—
0	$\frac{2}{\pi} \arcsin X$	$2/\pi$	0.24	0.52	0.71
1	$\frac{\operatorname{arctanh} X}{\operatorname{arctanh}(\cos i_{min})}$	$[\operatorname{arctanh}(\cos i_{min})]^{-1}$	0.17	0.38	0.53
2	$\frac{X}{\sqrt{1-X^2}} \tan i_{min}$	$\tan i_{min}$	0.14	0.31	0.44
3	$\frac{\operatorname{arctanh} X - \frac{X}{X^2-1}}{\operatorname{arctanh}(\cos i_{min}) + \cot i_{min} \csc i_{min}}$	$2[\operatorname{arctanh}(\cos i_{min}) + \cot i_{min} \csc i_{min}]^{-1}$	0.12	0.27	0.38

panels show the fractional error between the full analytical expressions and our Taylor approximations. The bottom panels indicate that the approximations are quite accurate for all but the smallest period orbits. In order to provide a more quantitative estimate of how well the Taylor expansions approximate the true posterior expressions, we provide in the right columns of Table 1 the values of prior transit probability X (or R_*/a for circular orbits) for which the Taylor approximations deviate from the analytical expressions for P_{tr} by 1%, 5%, and 10%. For $\alpha \leq 0$, the approximate transit probability expressions are accurate to within 10% for most values of X ; the 10% accuracy threshold moves to lower X with increasing α . For the eight transiting planets originally discovered by RV that were known at the time of pub-

lication, X ranges from ~ 0.015 for GJ 436 b to ~ 0.29 for 55 Cnc e, so the approximate transit probabilities for these planets have $< 10\%$ error (in fact, the approximations for all but 55 Cnc e are within a 5% error). If we can tolerate errors of one part in 10, we can confidently use these approximate posterior expressions for most situations.

5. POSTERIOR TRANSIT PROBABILITIES FOR MODEL PLANET MASS DISTRIBUTIONS

While the results from the previous section hold for power-law distributions, the true mass distribution of companions to stars of any type is not so well-behaved. For example, the brown dwarf desert is a well-known feature in the mass function of relatively short-period com-

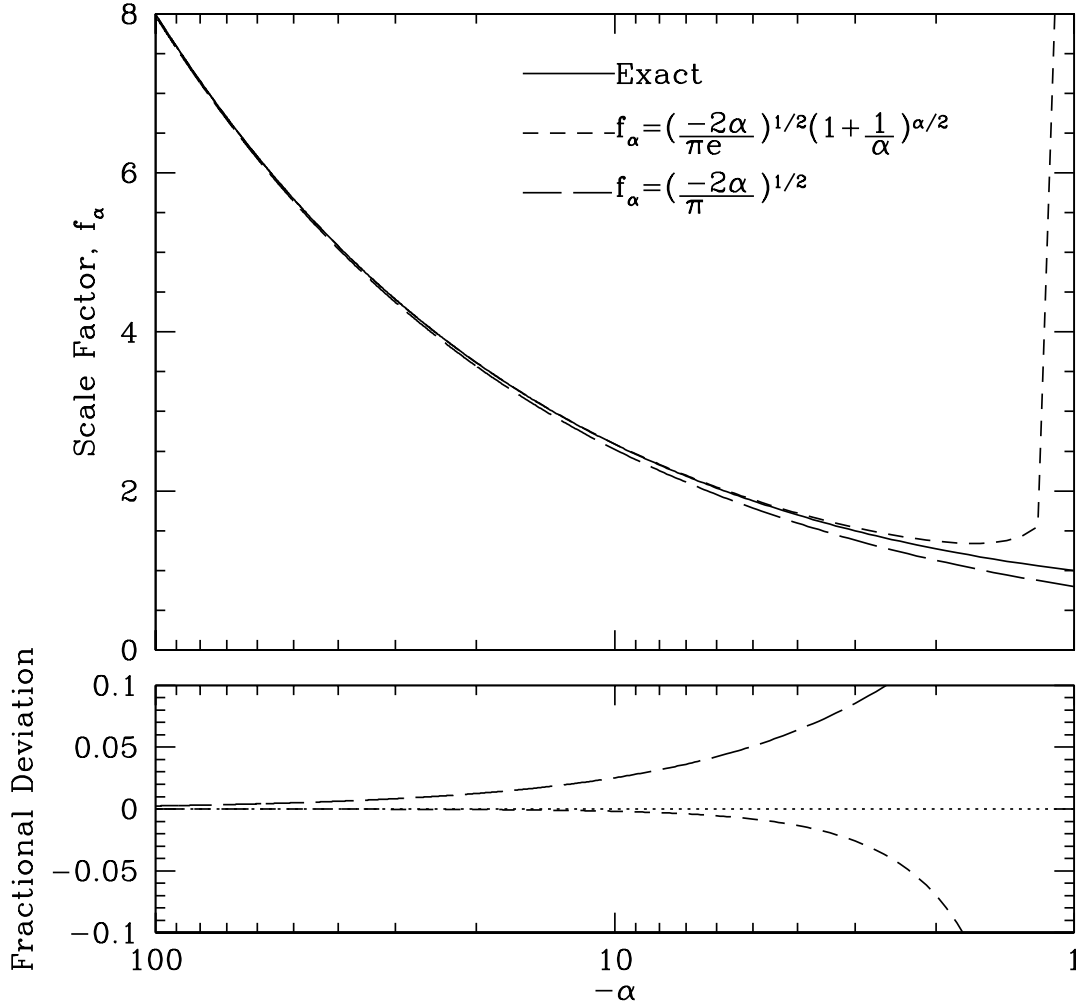


Figure 4. *Top panel:* The first-order posterior transit scaling factor f_α as a function of α for negative values of α . The solid line shows the exact expression obtained from numerical integration of Equation 23 with $\cos i_{\min} = 1$. The short-dashed line shows the approximation to f_α in Equation 25, whereas the long-dashed line shows the simpler approximation in Equation 26. *Bottom panel:* The fractional deviation of the approximations to f_α from the exact expression as a function of α .

panions to solar-type stars (Marcy & Butler 2000). It represents a local minimum in this mass function, with the frequency of companions rising toward the stellar regime on the high-mass side of the desert and toward the planetary regime on the low-mass side of the desert (Grether & Lineweaver 2006).

The biggest obstacle to providing robust a posteriori transit probabilities is that the mass distribution of planetary companions is poorly known. Radial velocity detections yield only the minimum mass of the companion, whereas planets discovered from ground-based transit surveys have severe and difficult-to-quantify selection biases (Pont et al. 2005; Gaudi et al. 2005; Gaudi 2005; Fressin et al. 2007). While Kepler has dramatically increased the number of known transiting planets, we do not have mass measurements for most of these systems.

We therefore adopt synthetic, but plausible, physically-motivated planetary companion mass distributions that

are derived from detailed planet formation simulations. We emphasize that we use these simply to illustrate the effects of more complicated mass functions on the transit probability; we do not claim to provide firm or robust predictions for these probabilities based on these mass functions.

We consider mass functions predicted by the planet formation models of Ida & Lin (2008) and Mordasini et al. (2012). To each of these, we also add stellar companions using a simple model based on the compilation of multiple stellar systems of Raghavan et al. (2010). Since the aridity of the brown dwarf desert is poorly constrained, we also consider two extreme variants of each mass function: one with brown dwarf companions with mass between the deuterium-burning and the hydrogen-burning limit as predicted by the planet formation theories, and one without such companions. We assume a deuterium-burning limit of $M \gtrsim 13M_{\text{Jup}}$ (Spiegel et al. 2011) and a

hydrogen-burning limit of $M \gtrsim 0.07M_{\odot}$ (Chabrier et al. 2000). We also assume all companions are on circular orbits. We discuss the determination of these mass distributions and analysis of the resulting posterior transit probability distributions in detail below.

5.1. Discussion of the True Mass Distributions

We took true masses of sub-stellar companions from the population synthesis models of Ida & Lin (2004) and Mordasini et al. (2012). Although the companion mass function in these models depends on the period, for simplicity we included all planetary companions, regardless of period.

For stellar-mass companions, we adopted a distribution based on the results of Grether & Lineweaver (2006) and Raghavan et al. (2010). Both groups examined a volume-limited sample of companions around Sun-like stars out to 25 pc from the *Hipparcos* catalog. Out to 25 pc, the mass ratio of the companions around Sun-like stars, M_c/M_* , is nearly flat over the linear mass ratio range 0.2-0.95 (Raghavan et al. 2010). Assuming that the host stars are all of solar mass, then the distribution of companion masses is approximately flat in M_c over the range $0.2M_{\odot} - 0.95M_{\odot}$. For simplicity, we set our mass distribution to be flat in M_c between $0.08M_{\odot}$ and $0.95M_{\odot}$.

We then combined the planetary and stellar mass distributions by normalizing the different mass regions, assuming that the planetary-mass companions from the model distributions with $1M_{\text{Jup}} \lesssim M_c \leq 13M_{\text{Jup}}$ are twice as common as stellar-mass companions around Sun-like stars (Grether & Lineweaver 2006). These combined mass distributions contain companions predicted by the planet formation models with masses in the brown dwarf regime. We also consider mass distributions with a completely arid brown dwarf desert. For these, we remove companions with masses between $13M_{\text{Jup}}$ and $0.07M_{\odot}$. Thus, we consider four different mass distributions: two with masses from Ida & Lin (2004) and two with masses from Mordasini et al. (2012), with one of each having a completely dry brown dwarf desert.

For each of these M_c distributions, we created a distribution of minimum masses M_0 as follows: For each true mass, we drew several values of $\cos i$ from a uniform distribution, transformed these to $\sin i$, and then multiplied each true mass by the $\sin i$ values to obtain minimum masses. Figure 5 show the final distributions of true and minimum masses, binned in in 0.25 dex bins in log mass. We show the distributions obtained from the two planet formation models, each with and without a completely dry brown dwarf desert. To guide the discussion, we have subdivided the mass function into several (somewhat arbitrary) regimes: sub-Earths ($10^{-8}M_{\oplus} - 0.1M_{\oplus}$), Earths/Super-Earths ($0.1M_{\oplus} - 10M_{\oplus}$), Neptunes ($10M_{\oplus} - 100M_{\oplus}$), Jupiters ($100M_{\oplus} - 10^3M_{\oplus}$), Super-Jupiters ($10^3M_{\oplus} - 13M_{\text{Jup}}$), brown dwarfs ($13M_{\text{Jup}} - 0.07M_{\odot}$) and stellar companions ($0.07M_{\odot} - 1M_{\odot}$).

The distributions all appear qualitatively similar and have several common features worth noting. In the stellar regime, the mass function falls toward lower masses as a power-law with a slope $\alpha \sim 0$ (by design). There is a local minimum in the brown dwarf regime, with

Table 2
Scale Factors for Model Mass Distributions with Brown Dwarf Companions

Regime	Mass Range	Ida & Lin ^a		Mordasini ^b	
		α	$\langle f \rangle$	α	$\langle f \rangle$
Earths/Super-Earths	$0.1M_{\oplus} - 10M_{\oplus}$	-1.5	1.12	-1.4	1.14
Neptunes	$10M_{\oplus} - 100M_{\oplus}$	-1.4	1.07	-1.7	1.19
Jupiters	$100M_{\oplus} - 10^3M_{\oplus}$	-0.9	0.99	-1.1	0.99
Super-Jupiters	$3M_{\text{Jup}} - 13M_{\text{Jup}}$	-2.2	1.42	-1.1	1.12
Brown Dwarfs	$13M_{\text{Jup}} - 0.07M_{\odot}$	-0.9	0.61	-1.5	0.86
Stars	$0.07M_{\odot} - 1M_{\odot}$	-0.2	1.80	-0.1	1.79

^aMass distribution using Ida & Lin companion masses.

^bMass distribution using Mordasini companion masses.

the mass function rising toward lower masses continuing into the planetary regime. In particular, there is a relatively sharp rise for Super-Jupiters, with the mass function roughly behaving as a power law with $\alpha \sim -2$ to $\alpha \sim -2.5$ in this regime. The mass function for Jupiters is essentially flat in $\log(M_c)$, i.e., $\alpha \sim -1$. For lower-mass planets, the mass function again begins to rise, with $\alpha \sim -1.5$ from the Neptune through the Earth/Super-Earth regime. Finally, the planet formation models predict a peak in the mass function at or below an Earth mass, with a fall off for companions less massive than this peak.

5.2. Posterior Transit Probability Calculations and Results

We can now use the companion M_0 values in the aforementioned mass distributions to estimate the posterior transit probabilities for planets in bins of M_0 . To proceed, we assume that the host star is a solar radius and that the companion orbits with a semimajor axis of 0.1 AU. We then calculate the transit probability of each M_0 bin by examining the fraction of companions in that bin that transit — i.e. the fraction for which $\cos i \leq R_{\odot}/(0.1 \text{ AU})$. We then normalized the transit probability to the a priori transit probability $R_{\odot}/(0.1 \text{ AU})$, thereby providing an estimate of the factor f by which the a posteriori transit probability is scaled relative to the prior transit probability, in analogy to f_{α} for the power-law mass function priors.

We plot the scale factor against mass in Figure 6. For most mass ranges, the scale factor f for a given $M_c \sin i$ differs little between the different mass distributions, with the most pronounced discrepancy happening in the brown dwarf regime below the deuterium-burning limit. In Table 2, we list the average scale factor values in each mass regime for the two mass distributions with brown dwarfs. There are several important points to note about the distribution of scale factors.

- In the Jupiter mass regime ($100M_{\oplus} - 10^3M_{\oplus}$), the slope of the mass distribution is reasonably well-approximated by a power-law with index $\alpha \approx -1$, so $f_{-1} = 1$ and the prior and posterior transit probabilities are very similar. Consequently, using the posterior probability in this mass regime, rather than the prior, would not substantially change target selection criteria for transit follow-up observations (assuming the prior on the mass function in this regime is realistic).
- In the Super-Jupiter regime ($3M_{\text{Jup}} - 13M_{\text{Jup}}$), the

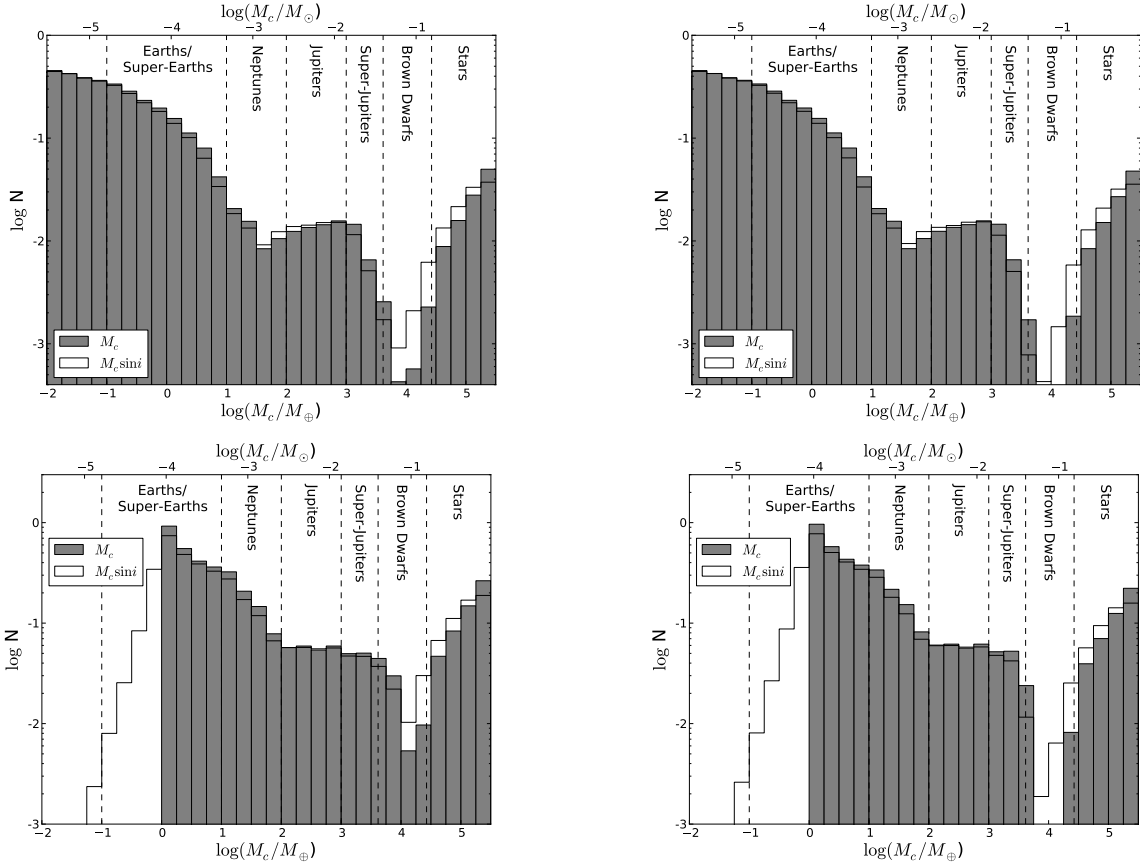


Figure 5. Mass distributions of companions around Sun-like stars using planetary companions from Ida & Lin (top) and Mordasini (bottom), with (left) and without (right) brown dwarf companions in the deuterium-burning to hydrogen-burning mass range. The true mass distributions are shown as filled histograms, whereas the minimum mass distributions are outlined. The vertical dashed lines divide the plots into the sub-Earth, Earth/Super-Earth, Neptune, Jupiter, Super-Jupiter, Brown Dwarf and stellar mass regimes as described in the text. Values of α for the various regimes are as follows, starting with Earths/Super-Earths and increasing in mass: $\alpha \approx -1.5, -1.4, -0.9, -2.2, -0.9, \text{ and } -0.2$ for the top-left panel; $\alpha \approx -1.5, -1.4, -0.9, -2.5, -0.8, \text{ and } -0.1$ for the top-right panel; $\alpha \approx -1.4, -1.7, -1.1, -1.1, -1.5, \text{ and } -0.1$ for the bottom-left panel; and $\alpha \approx -1.4, -1.7, -1.1, -1.6, -1.3, \text{ and } -0.1$ for the bottom-right panel.

transit probabilities are boosted by $\sim 20 - 50\%$.

- The posterior transit probabilities for Neptunes and Super-Earths are also boosted relative to the prior transit probabilities.
- The posterior transit probabilities for companions with minimum mass near the high-mass end of the brown dwarf desert have very low posterior transit probabilities and are thus poor targets for transit follow-up searches. These systems are simply much more likely to be low-mass stars seen at relatively low inclination angle i .

Together, these results suggest that RV detected planets with $M_c \sin i$ in the mass range of Earths, Super-Earths, Neptunes, or Super-Jupiters are generally better-than-expected targets for transit follow-up, whereas companions in the BD desert are poor targets for transit follow-up.

6. APPLICATION TO KNOWN RV SYSTEMS: IDENTIFYING PROMISING SYSTEMS FOR PHOTOMETRIC FOLLOW-UP

In this section, we apply the posterior transit probabilities derived from our model mass distributions to

known RV planets in order to identify specific systems that might be significantly better candidates for transit follow-up observations than would be expected based on the naive prior transit probability.

Before doing so, however, it is worth asking whether or not there is any evidence that the planet mass distributions we have adopted have any correspondence to the true mass distribution of planetary companions (c.f. Mordasini et al. 2009).

Estimates of the true mass distribution of Jupiter-mass planets discovered by RV surveys generally find distributions that are roughly flat in $\log M_c$ (e.g. Watson et al. 2010), consistent with mass functions used here and suggesting that the posterior and prior transit probabilities for such companions should be similar. It is worth noting that the first transiting planet, HD 209458 b (Charbonneau et al. 2000; Henry et al. 2000), was found “right on time” based on adopting the prior transit probability for hot Jupiters of $\sim 10\%$, and given the ~ 10 hot Jupiter systems that were known at the time.

It is also interesting to note that there are two transiting Super-Jupiters and three transiting Jupiters among the planets orbiting solar-type stars that were originally discovered by RV, despite the fact that super-Jupiters are much rarer than Jupiter-mass companions among short-

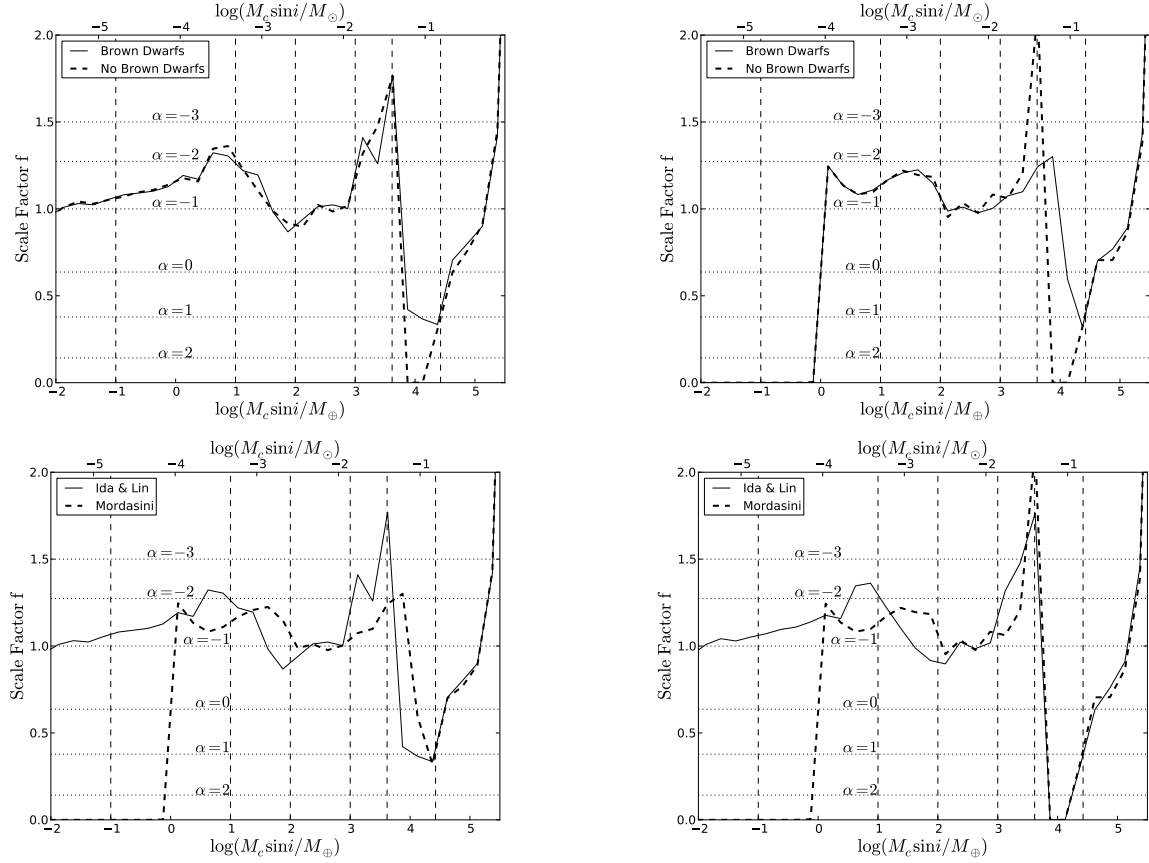


Figure 6. Scale factors f (ratio of posterior to prior transit probability) as a function of minimum companion mass for the model mass distributions. The upper-left panel corresponds to the distributions with Ida & Lin planetary masses while the upper-right panel corresponds to Mordasini planetary masses. The bottom panels compare scale factors as a function of mass between the Ida & Lin and Mordasini distributions with (bottom-left) and without (bottom-right) brown dwarfs.

period systems. This is consistent with the prediction of the mass functions adopted here that the posterior transit probability of Super-Jupiters is higher than the posterior transit probability of Jupiters.

While this anecdotal evidence based on the rates of transiting Jupiters and Super-Jupiters is intriguing, there are of course other factors that strongly affect the transit probability, including the semimajor axis, argument of periastron, and host radius. To account for these effects, we compared the number of RV-detected planets that have been identified to transit to the expected number of transiting planets based on the naive prior transit probability. We took our exoplanet sample from the Exoplanet Orbit Database on 19 April 2013 (Wright et al. 2011). We included only the 380 RV planets in the database whose eccentricity e , semimajor axis a , angle of periastron ω and host star’s radius R_* were listed. We also included the eight planets first detected by RV and subsequently found to transit. For each RV planet, we found the prior transit probability from its orbital parameters and using the general form of the prior transit probability given in Equation (9), assuming $R_* \gg R_c$. We then partitioned the planets into three 1-dex bins of $\log(M_c \sin i)$. We estimated the expected number of transits in each bin by adding the prior transit probabilities of the planets in that bin. We divided the actual number of transiting planets in each bin by the predicted number of transiting planets.

This ratio of the number of known transiting planets to the number predicted based on the prior transit probability is shown in Figure 7. Note that the ratio plotted is strictly a lower limit to the actual ratio of transiting planets to predicted number of transiting planets, since there may exist transiting planets among the sample of RV detected systems that have not yet been identified to transit. In particular, identifying or definitively excluding transits of long period systems is quite difficult because of the infrequent transit opportunities and generally large uncertainties in the predicted times of inferior conjunction. With this in mind, we also show the ratio after restricting to RV systems with semimajor axes $a \leq 0.5$ AU and $a \leq 0.2$ AU. Presumably, the systems in these subsets have been more thoroughly vetted for transits, and thus the sample of transiting planets is more nearly complete. Because of the small number of known transiting systems and the likely incompleteness, we caution against drawing any strong conclusions. Nevertheless, for the bins in which there are a non-zero number of known transiting systems, the results are generally consistent with the expectations from the mass functions adopted here. In particular, the observed number of transiting planets with minimum mass between M_{Jup} and $10M_{Jup}$ ($M_c \sin i = 10^{2.5}M_\oplus - 10^{3.5}M_\oplus$) transiting planets is apparently higher than one would expect based on the naive prior transit probability.

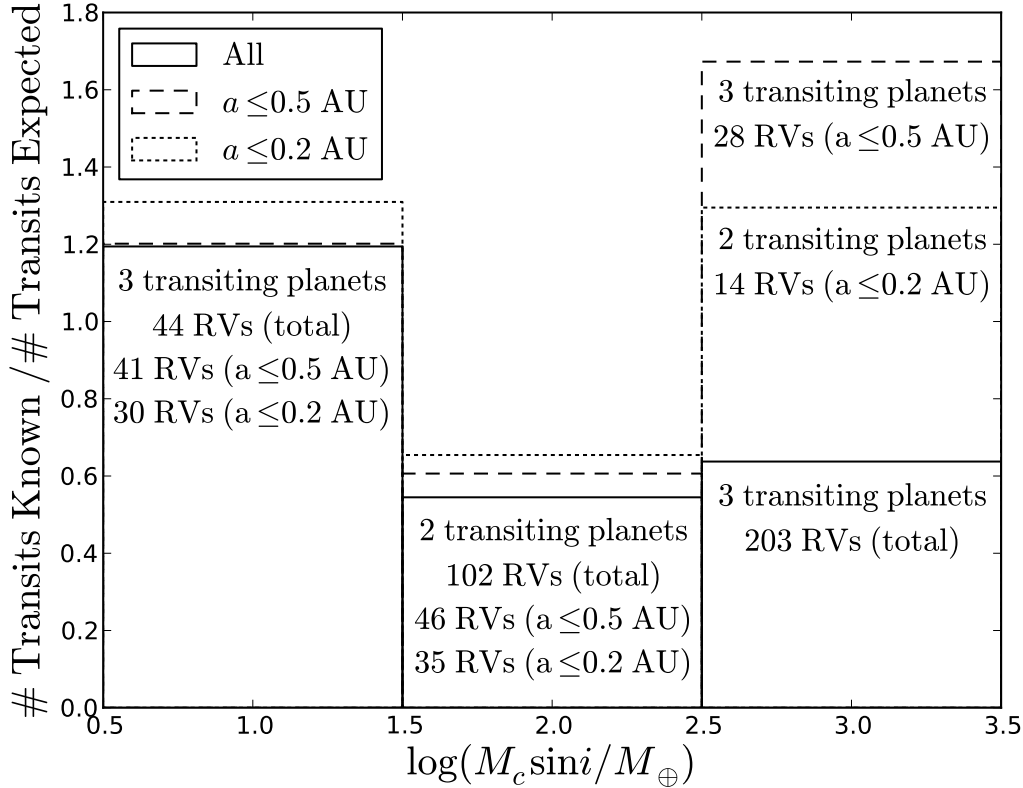


Figure 7. The ratio of transits to the expected number of transits as a function of $M_c \sin i$, plotted for all planets in the sample (solid line), planets with semimajor axes $a \leq 0.5$ AU (dashed line) and planets with semimajor axes $a \leq 0.2$ AU (dotted line).

6.1. Posterior-Prior Comparison and Transit Candidate Identification

To compare the prior and posterior transit probabilities for known RV planets, in Figure 8 we plot the posterior probability versus T , following Kane & Von Braun (2008), as well as the ratio of the posterior and prior transit probabilities. The prior transit probabilities were estimated with Equation 9 assuming $R_p \ll R_*$, the values of e , ω , R_* , M_* , and a as given by the Exoplanets Orbit Database.³ We determine posterior transit probability scalings using both the Ida & Lin and Mordasini model mass distributions that include brown dwarfs. To find the posterior transit probability scaling for a given RV system, we simply choose the value of the posterior transit probability scaling for the 0.25 dex bin in $\log(M_c \sin i)$ in which the RV companion is located in Figure 5.

The overall trend of the transit probabilities versus T is similar for all cases, and simply reflects the scaling $P_{tr} \propto X \propto T^{-2/3}$. To guide the eye, in Figure 8 we plot the simple prior transit probability for circular orbits, a star with a solar density, and a planet with a small mass and radius compared to the star: $P_{tr,0} = (3\pi/G)^{1/3} \rho_\odot^{-1/3} T^{-2/3}$. Deviations from this fiducial probability are due to eccentricity, orientation of the orbit (ω), variations in ρ_* , and finally, in the case of the

posterior probabilities, variations in the posterior scaling factor. The vertical grouping of systems with large periods ($10^2 \text{ days} \lesssim T \lesssim 10^3 \text{ days}$) and relatively large transit probabilities are planets orbiting giant stars with large radii. Although the transit probabilities are large for these systems, any transits in such systems would be very shallow and very long. Specialized methods are generally needed to detect such transits; these are discussed in detail in Assef et al. (2009).

The transit scale factor (ratio of posterior to prior transit probabilities) inferred from the Ida & Lin model shows considerably more variance than that inferred from the Mordasini model. This simply reflects fact that the Mordasini mass distribution is smoother than that of the Ida & Lin distribution in the planetary regime (see Fig. 5). Also, because the Mordasini distribution of companion masses increases nearly monotonically toward lower mass down to $\sim M_\oplus$, the scale factors inferred from this model are never substantially less than unity for the known exoplanets. On the other hand, the Ida & Lin mass distribution shows a clear local minimum near $\sim 30 M_\oplus$ (a consequence of the “planet desert” discussed in Ida & Lin 2004), and therefore the inferred scale factors for planets with minimum mass somewhat larger than this minimum are significantly less than unity. For the Ida & Lin model, we find that the posterior probability is less than the prior probability for $\sim 19\%$ the planets in the sample, as opposed to $\sim 34\%$ for the Mordasini distribution.

More interesting, however, is the fact that we infer a

³ The semimajor axes in this database were derived using Kepler’s Third Law and assuming that the true companion mass is equal to its minimum mass (Butler et al. 2006; Wright et al. 2011)

posterior probability that is markedly higher for some planets, particularly for the Ida & Lin model. These are the ones we will focus on here. To identify such promising transit candidates, we begin by eliminating giant star hosts with $R_* > 2.5R_\odot$ (marked with plus signs in Figure 8) from consideration. From the remaining planets, we choose planets from either model that have both a high posterior transit probability of $P_{tr} \geq 0.1$, and a high prior transit scale factor of $f \geq 1.2$, i.e. for which $P_{tr} > 1.2P_{tr,0}$. These planets lie above the dotted lines in both the top and bottom panels of Figure 8, and are marked with an X.

These cuts leave us with a sample of fourteen planets, which are listed in Table 3. Thirteen planets pass the cuts from the Ida & Lin distribution, whereas only HD 47186 b passes from the Mordasini distribution. None of the candidates pass the cuts from both distributions. Among these fourteen, 55 Cnc e and HD 17156 b have already been shown to transit, whereas transits in HD 40306 b, HIP 14810 b, and τ Boo b have been conclusively ruled out. The sum of the posterior transit probabilities of the remaining candidates is ~ 1.15 , suggesting that one transiting system may lurk amongst these systems. Detecting or excluding transits from most of these systems will be challenging from the ground, as most have predicted depths of $\sim 0.05 - 0.1\%$, based on the minimum mass and a mass/radius relation of $R_c = R_\oplus (M_c/M_\oplus)^{0.53}$ (Weiss et al. 2013).

7. ADDITIONAL ISSUES AFFECTING THE TRANSIT PROBABILITY

We now turn our attention to two issues that, to our knowledge, have not been previously discussed and can, in principle, subtly affect transit probability estimates. First, we consider the uncertainty in the transit probability arising from uncertainties in the input parameters that are used to estimate the transit probability. Second, we consider the effect of the dependence of the semimajor axis (and so the transit probability) on the orbital inclination. In both instances, we find that the quantitative changes to the estimated transit probability are likely to be negligible in most instances, although they can be larger and therefore more important in some special cases.

We begin by writing down the expression for the posterior transit probability in the limit of small transit probabilities (i.e., $X \ll 1$), in which case we can write P_{tr} as a constant factor f times the prior transit probability,⁴

$$P_{tr} \simeq fX = f \frac{R_* + R_c}{a} g(e, \omega). \quad (27)$$

where we have defined

$$g(e, \omega) \equiv \frac{1 + e \sin \omega}{1 - e^2}. \quad (28)$$

It is instructive to deconstruct this expression for the transit probability in terms of the quantities that can be measured directly from the RV data and those that must be inferred or assumed from external information. The relevant RV observables are T , e , and ω . Using Newton's

form of Kepler's Third law and defining the bulk density of the star $\rho_* \equiv 3M_*/(4\pi R_*^3)$, the transit probability can be written as

$$P_{tr} = \left(\frac{3\pi}{G} \right)^{1/3} f \rho_*^{-1/3} (1+q)^{-1/3} (1+r) T^{-2/3} g(e, \omega), \quad (29)$$

where we have defined the mass ratio $q \equiv M_c/M_*$ and the radius ratio $r \equiv R_c/R_*$. Thus, in the limit that $r \ll 1$ and $q \ll 1$ the only parameter of the star that enters into the transit probability is the density ρ_* . In fact, one can write,

$$P_{tr} = (3\pi)^{1/3} f (1+q)^{-1/3} (1+r) \left(\frac{t_{dyn}}{T} \right)^{-2/3} g(e, \omega), \quad (30)$$

suggesting that the more fundamental physical quantity is, in fact, the free-fall or dynamical time of the star $t_{dyn} \equiv (G\rho_*)^{-1/2}$.

It is useful to examine and classify the parameters that enter into Equation (29). The RV observables T , e , and ω will have uncertainties associated with them, and these uncertainties may be correlated. The stellar density ρ_* must be inferred from external information, i.e. from the stellar temperature, surface gravity, and metallicity derived from a high-resolution spectrum (perhaps combined with a parallax measurement) or directly from astroseismology. Both the RV parameters and stellar densities will have measurement uncertainties associated with them. We discuss the effect of these uncertainties in Section 7.1. Finally, the posterior scaling factor f and the radius ratio r must simply be assumed. These may be uncertain, but these are not statistical uncertainties in the traditional sense; rather, they are systematic uncertainties associated with the prior. We will not consider these further. The last parameter, q , arises from the fact that the period T is observed but it is the semimajor axis that determines the transit probability. In fact, the companion mass M_c has a definite value at the inclination at which transits occur, and so this can be determined. We explore this latter issue in Section 7.2.

7.1. Measurement Uncertainties

Discussion of transit probabilities — prior or otherwise — is often unaccompanied by any discussion of the uncertainties in the measurements of the relevant orbital parameters. Consider Equation (29), which can be rewritten as $\log P_{tr} = \log f + \log(1+r) - \frac{1}{3} \log(1+q) - \frac{1}{3} \log \rho_* - \frac{2}{3} \log T + \log g(e, \sin \omega) + \text{const}$. Again, we will ignore the uncertainty in f and r here, and we discuss the effect of q in the next section. The uncertainty in the transit probability $\sigma_{P_{tr}}$ due to uncertainties in the remaining quantities is

$$\left(\frac{\sigma_{P_{tr,0}}}{P_{tr,0}} \right)^2 = \frac{1}{9} \left(\frac{\sigma_{\rho_*}}{\rho_*} \right)^2 + \frac{4}{9} \left(\frac{\sigma_T}{T} \right)^2 + \left(\frac{\sigma_{g(e, \sin \omega)}}{g(e, \sin \omega)} \right)^2, \quad (31)$$

where we have assumed that the uncertainties in ρ_* , T , and (e, ω) are uncorrelated, which is generally a good assumption. We note that uncertainty in the transit probability depends fairly weakly on the stellar density ρ_* . Furthermore, the period T is usually comparatively well-measured, so despite the higher intrinsic sensitivity

⁴ Formally, we only demonstrated this to be true for power-law priors for M_c , but we expect it to be generally true for any prior that is smooth at $M_c = M_0$.

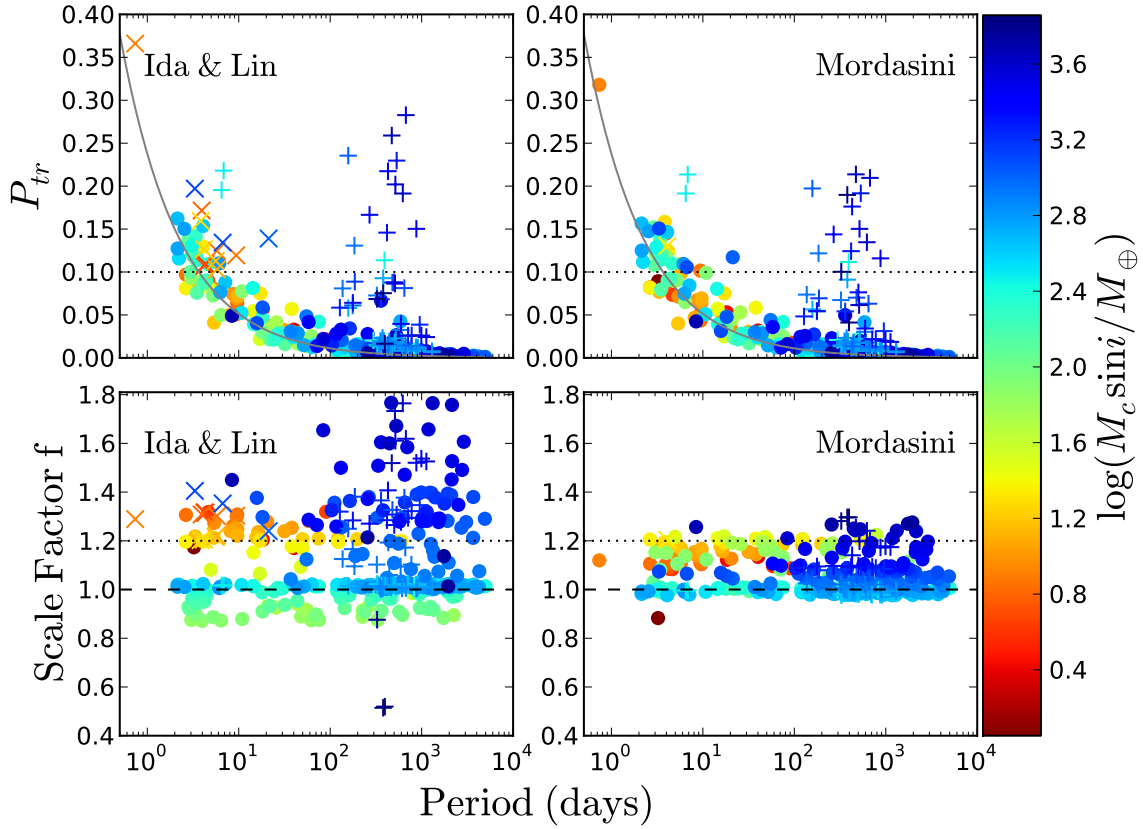


Figure 8. *Top panels:* Posterior probability as determined using the Ida & Lin mass distribution (left) and Mordasini distribution (right) for RV-detected planets that have a full list of orbital parameters in the Exoplanets.org Database. The solid grey line shows the simple prior transit probability for circular orbits, a star with a solar density, and a planet with a small mass and radius compared to the star. The dotted line marks posterior transit probabilities above 10%. *Bottom panels:* Scale factors for the same planets. The dashed line denotes a posterior probability equal to the prior, while the dotted line denotes a posterior that has a 20% boost relative to the prior. In all panels, bluer colors mark more massive planets, a plus sign denotes planets whose host stars have $R_* \geq 2R_\odot$ and X marks planets that have $P_{tr} \geq 0.1$ and $f_\alpha \geq 1.2$; the latter are listed in Table 3

Table 3
Transiting Planet Candidates

Name	$M_c \sin i (M_{\text{Jup}})$	Period (days)	$M_* (M_\odot)$	$R_* (R_\odot)$	V (mag)	Transit Depth ^a	P_{tr}	$P_{tr,0}$	f_α
61 Vir b	0.016	4.215	0.942	0.980	4.9	4.92×10^{-4}	0.107	0.081	1.317
BD -08 2823 b	0.046	5.600	0.740	1.279	10	8.82×10^{-4}	0.113	0.093	1.216
HD 10180 c	0.042	5.760	1.060	1.109	7.3	1.05×10^{-3}	0.103	0.084	1.221
HD 125612 c	0.058	4.155	0.902	1.043	9.0	1.70×10^{-3}	0.126	0.105	1.206
HD 1461 b ^b	0.024	5.773	1.026	1.130	6.6	5.67×10^{-4}	0.125	0.096	1.302
HD 181433 b	0.024	9.374	0.8	1.008	8.4	7.03×10^{-4}	0.119	0.092	1.304
HD 215497 b	0.021	3.934	0.872	1.107	9.1	5.10×10^{-4}	0.172	0.131	1.308
HD 219828 b	0.062	3.834	1.24	1.468	8.0	9.24×10^{-4}	0.159	0.133	1.203
HD 47186 b ^c	0.071	4.085	1.0	1.131	7.6	1.79×10^{-3}	0.130	0.108	1.204
55 Cnc e ^d	0.026	0.737	0.905	0.943	6.0	4.54×10^{-4}	0.366	0.284	1.289
HD 17156 b ^d	3.30	21.217	1.285	1.507	8.2	5.29×10^{-3}	0.139	0.112	1.240
HD 40307 b ^e	0.013	4.312	0.740	0.839	7.2	5.33×10^{-4}	0.109	0.083	1.315
HIP 14810 b ^e	3.87	6.674	0.990	1.320	8.5	9.11×10^{-2}	0.134	0.099	1.353
τ Boo b ^e	4.17	3.312	1.341	1.418	4.5	8.52×10^{-2}	0.197	0.140	1.405

^aTransit depth $(R_c/R_*)^2$, assuming the minimum mass and a mass-radius relation $R_c = R_\oplus (M_c/M_\oplus)^{0.53}$ (Weiss et al. 2013).

^bRivera et al. (2010) did not definitively rule out transit.

^cCandidate using posterior from Mordasini mass distribution.

^dKnown transiting planet.

^eTransits excluded.

of P_{tr} to it, it generally contributes negligibly to the total uncertainty.

Turning to e and ω , we note that the expression for $\sigma_{g(e, \sin \omega)}$ depends on the covariance of e and ω . For simplicity, we consider only the limit in which these parameters are uncorrelated:

$$\left(\frac{\sigma_{g(e, \sin \omega)}}{g(e, \sin \omega)} \right)^2 \approx E\sigma_e^2 + \Omega\sigma_\omega^2, \quad (32)$$

where we have defined

$$E \equiv \frac{4e^2}{(1-e^2)^2} + \frac{\sin^2 \omega}{(1+e \sin \omega)^2} \quad (33)$$

and

$$\Omega \equiv \left[\frac{e \cos \omega}{1+e \sin \omega} \right]^2. \quad (34)$$

Figure 9 shows the prefactors E and Ω as a function of e and ω .

It is instructive to consider the behavior of E and Ω in the limit of $e \ll 1$. To first order in e , we have that $E \simeq \sin^2 \omega - 2e \sin^3 \omega$. For $\omega = 0$ and $\omega = \pi$, i.e. orbits such that the semimajor axis is perpendicular to the line of sight, the contribution of the eccentricity to the uncertainty in P_{tr} vanishes. In addition, for $e = 0$, there is a finite contribution to the uncertainty in P_{tr} for all values of ω except 0 and π , reaching a maximum of $E = 1$ for $\omega = \pi/2$ or $3\pi/2$; these values correspond to orbits such that the semimajor axis is along the line of sight. With regards to Ω , there is no contribution to the uncertainty in P_{tr} to first order in e , and we can therefore expect the contribution of the uncertainty in e to dominate over that of ω . We conclude that for small e , uncertainties in e and ω generally do not lead to large uncertainties in P_{tr} , with the contribution to the fractional uncertainty in P_{tr} at most of order σ_e .

On the other hand, for orbits with large eccentricity, the uncertainties in e and ω can have a substantial effect on the uncertainty in the transit probability. First consider the full expression for E . It is clear that since both terms are positive and the first term in E does not depend on ω , E is minimized at $\omega = 0$ for all e . Furthermore, E diverges as $e \rightarrow 1$ for all ω . Next, consider the full expression for Ω . The contribution of ω to the uncertainty vanishes for $\omega = \pi/2$ or $3\pi/2$, regardless of eccentricity. Ω is maximized at $\omega = \pi + \arcsin e$ and $\omega = 2\pi - \arcsin e$, with maximum value of $\Omega_{max} = e^2/(1-e^2)$ that diverges as $e \rightarrow 1$.

7.2. True versus Minimum Semimajor Axis

In order to estimate the transit probability, one needs an estimate of the true semimajor axis. However, one measures only the period T and the mass function \mathcal{M} . These, together with an estimate of M_* , only allow one to measure a *minimum* semimajor axis a_{min} . This minimum semimajor axis can be determined by first using the expression for the mass function (Equation 3) to determine the minimum companion mass $M_{c,min}$ for $\sin i = 1$, and then using this to solve for a using Newton's version of Kepler's Third Law (Equation 4). Since a_{min} is the minimum semimajor axis, the transit probability estimated in this way will be an overestimate of the true transit probability.

Since the expression for a_{min} is complicated, we will consider a somewhat simpler estimate for a ,

$$a_0 \equiv \left(\frac{GM_*}{4\pi^2} \right)^{1/3} T^{2/3} = a(1+q)^{-1/3}. \quad (35)$$

The relation between the transit probability P_{tr,a_0} estimated using a_0 and the true transit probability is

$$P_{tr} = P_{tr,a_0}(1+q)^{-1/3} \simeq P_{tr,a_0} \left(1 - \frac{1}{3}q \right), \quad (36)$$

where the rightmost expression holds for $q \ll 1$. Thus, for small q , the fractional amount by which one overestimates the transit probability using a_0 is $\sim q/3$. For a Jupiter-mass companion, this is only $\sim 0.03\%$ — essentially negligible. For a companion at the hydrogen-burning limit, the error is 2.5%. Of course, one does not know the mass of the companion *a priori*.

Although the amount by which one overestimates the transit probability is generally negligible, the true transit probability can nevertheless be determined with no approximation. This is accomplished by solving for the value of q at the critical inclination for a transit i_{min} , and then using this value of q to determine the true semimajor axis. We proceed by defining

$$Q \equiv \frac{\mathcal{M}}{M_*} = \frac{q}{(1+q)^{2/3}} (1 - \cos^2 i)^{1/2}, \quad (37)$$

which we call the “mass ratio function” in analogy to the mass function. The true transit probability at the critical inclination is simply the cosine of the critical inclination, i.e., $P_{tr} = \cos i_{min} = P_{tr,a_0}(1+q)^{-1/3}$. We can then insert this expression for $\cos i_{min}$ into Equation (37) and, by defining $y \equiv 1+q$, derive a polynomial equation in y when $i = i_{min}$:

$$Q^2 y^2 - (y-1)^2 (y^{2/3} - P_{tr,a_0}^2) = 0. \quad (38)$$

Recall that Q and P_{tr,a_0} are observables. This expression can be solved for y with standard techniques.

Figure 10 shows $P_{tr}/P_{tr,a_0} = y^{-1/3}$ as functions of Q and P_{tr,a_0} . For typical prior transit probabilities, P_0 overestimates the actual prior transit probability by less than 10% over the entire range of Q . Note that, in the limit that $q \ll 1$,

$$q \simeq Q(1 - P_{tr,a_0}^2)^{-1/2}. \quad (39)$$

In the right panel of Figure 10, for $P_{tr,a_0} \ll 1$, $P_{tr}/P_{tr,a_0} \simeq 1 - Q/3$.

8. SUMMARY AND CONCLUSION

We have derived a general expression for the *posterior* probability that a radial velocity companion with minimum mass $M_0 = M_c \sin i$ also transits its parent star. The posterior transit probability depends on both the prior distribution of the orbital inclination angle i and the prior distribution of the true companion mass M_c . We evaluated this expression for power-law distributions of M_c and integer power-law indices $-3 \leq \alpha \leq 3$, deriving exact analytic expressions for the posterior transit probability for these cases. We found that, for power-law distributions in general, the posterior transit probability is well-approximated

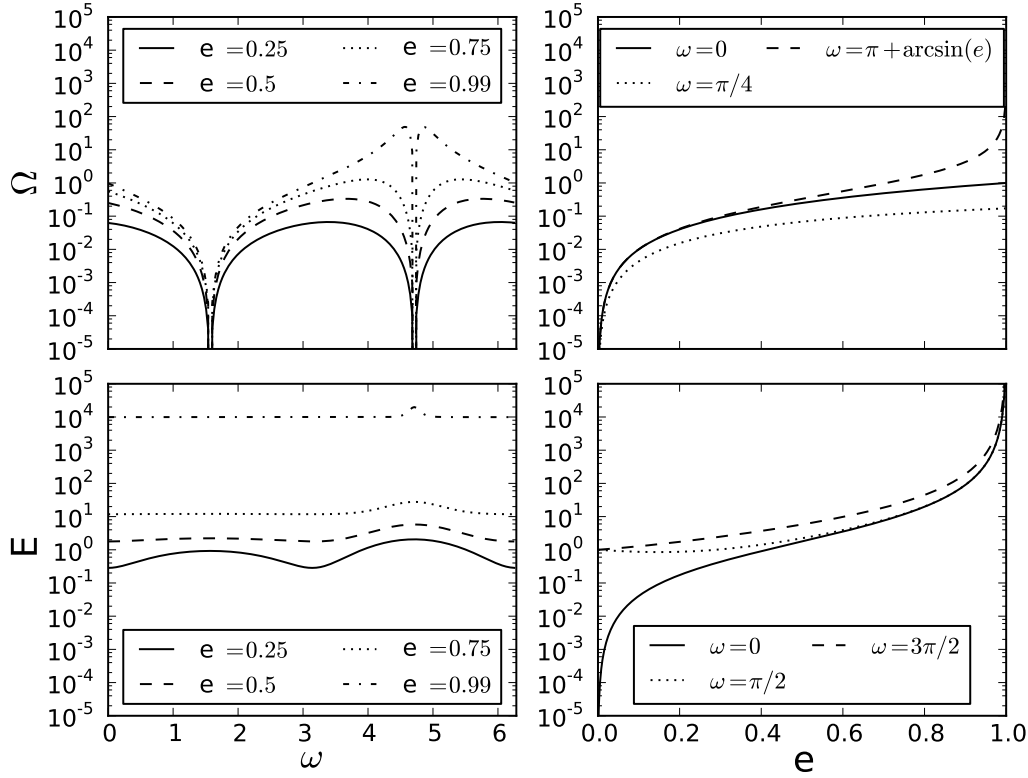


Figure 9. Contributions to the transit probability error from Ω (top) and E (bottom) as functions of ω (left) and e (right) in the uncorrelated limit.

as a scalar multiple f_α of the prior probability, with specific values $f_{-3} = 3/2$, $f_{-2} = 4/\pi$, $f_{-1} = 1$, $f_0 = 2/\pi$, $f_1 = 1/\text{arctanh}(\cos i_{\min})$, $f_2 = \tan i_{\min}$, and $f_3 = 2/[\text{arctanh}(\cos i_{\min}) + \cot(i_{\min}) \csc(i_{\min})]$, where i_{\min} is the minimum inclination angle corresponding to the maximum companion mass such that $M_{c,\max}/M_0 = 1/\sin i_{\min}$. For $\alpha \ll 0$, $f_\alpha \sim (-2\alpha/\pi)^{1/2}$.

We then applied our findings to four synthetic but physically motivated companion mass distributions. In all four cases, we find that $\alpha \simeq -1$ for Jupiters ($100M_\oplus - 10^3M_\oplus$), and therefore the prior and posterior probabilities are very similar. On the other hand, we find $\alpha \simeq -1.5$ for Earths and Super-Earths ($0.1M_\oplus - 10M_\oplus$), and $\alpha \simeq -2$ to -2.5 for Super-Jupiters ($10^3M_\oplus - 13M_{\text{Jup}}$). The posterior transit probability for RV planets with masses in these regimes is therefore boosted relative to the prior, so we may expect more transiting planets in these mass regimes. With transit surveys pushing well into the Super-Earth regime, this result is encouraging.

For brown dwarfs ($13M_{\text{Jup}} - 0.07M_\odot$), the scale factor of the posterior transit probability relative to the prior depends in detail on the aridity of the brown dwarf desert, as well as on the precise value of the minimum mass that is measured. In general, the scale factor drops as one moves from the Super-Jupiter up through the brown dwarf mass regime. In particular, objects with minimum mass just above the driest part of the brown dwarf desert may have strongly suppressed transit probabilities, since such an object is more likely a

stellar-mass companion being viewed pole-on than a true brown dwarf. For stellar companions, ($0.07M_\odot - 1M_\odot$), $\alpha \approx 0$, and thus the posterior transit probability is generally smaller than the prior probability in this regime.

Using these mass distributions and the corresponding scale factors, we estimated posterior transit probabilities for RV-discovered planets in the Exoplanets.org Database (Wright et al. 2011). Selecting planets for which the posterior transit probability is $> 10\%$ and $> 20\%$ larger than the prior probability, excluding companions around giants, known transiting planets, and planets for which transits have been ruled out, we found nine particularly promising transiting planet candidates: 61 Vir b, BD -08 2823 b, HD 10180c, HD 125612 c, HD 1461 b, HD 181433 b, HD 215497 b, HD 219828 b, and HD 47186 b.

Finally, we discuss two issues that can subtly affect the calculation of either the posterior or the prior transit probability. We find that uncertainties in the eccentricity e and argument of periastron ω generally do not yield significant uncertainties in the transit probability, provided e is small. However, measurement uncertainties in e and ω for companions in highly-eccentric orbits can have a significant impact on the transit probability, with the uncertainty in e being amplified by a factor that diverges as $e \rightarrow 1$ for all ω , and the uncertainty in ω being amplified by a factor that also diverges with increasing e for the specific case of $\omega = \pi + \arcsin(e)$. Additionally, we point out that the semimajor axis typically used in determining the transit probability is typically smaller

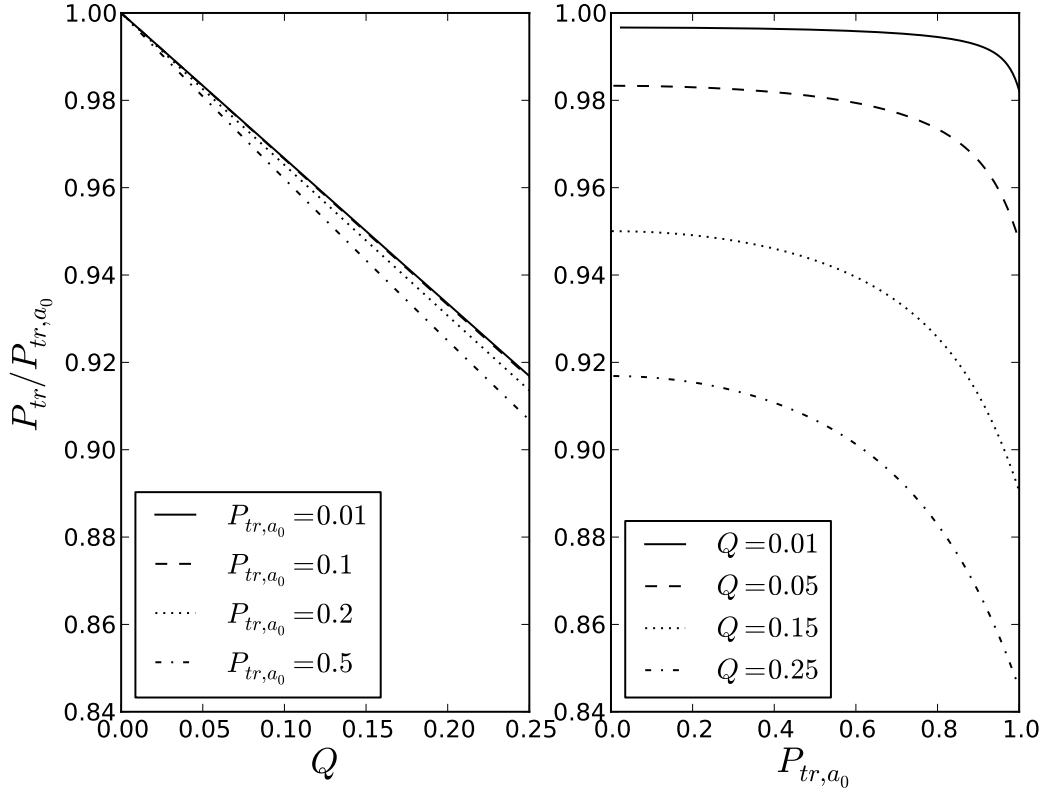


Figure 10. Comparison of the actual prior transit probability, P_{tr} , and the prior transit probability calculated with a_0 , P_{tr,a_0} , plotted against the “mass function ratio” Q (left) and P_{tr,a_0} (right). For reasonable values of P_{tr,a_0} ($\lesssim 0.5$), using a_0 leads to overestimation of the prior by no more than 10% over the entire range of Q .

than the true semimajor axis, which leads to an overestimate of the true probability. We demonstrate that this overestimate is negligible for systems with small transit probabilities, but becomes more significant as the transit probability approaches unity.

The primary difficulty with estimating the posterior transit probability is that the mass distribution of low-mass companions is poorly known. Nevertheless, even the theoretical distributions we studied here likely provide a more accurate estimate than the naive prior transit probability. These distributions suggest that RV companions with minimum masses in the Earth/Super-Earth and Super-Jupiter regimes are promising targets for transit follow-up. As measurements of the companion mass distribution become increasingly robust, we look forward to more frequent use of the posterior transit probability — accompanied, of course, by an appropriate discussion of assumptions, priors, and sources of uncertainty.

We thank Shigeru Ida and Christoph Mordasini for allowing us to use results from their planetary formation models in our posterior transit probability calculations. We also thank Thomas Beatty, Christian Clanton, Calen Henderson, Matthew Penny, and Tim Morton for their helpful discussions and suggestions. This research has made use of the Exoplanet Orbit Database and the Exoplanet Data Explorer at exoplanets.org.

REFERENCES

- Alonso, R., Brown, T. M., Torres, G., et al. 2004, *ApJ*, 613, L153
 Alsubai, K. A., Parley, N. R., Bramich, D. M., et al. 2011, *MNRAS*, 417, 709
 Assef, R. J., Gaudi, B. S., & Stanek, K. Z. 2009, *ApJ*, 701, 1616
 Bakos, G. Á., Noyes, R. W., Kovács, G., et al. 2007, *ApJ*, 656, 552
 Barbieri, M., Alonso, R., Laughlin, G., et al. 2007, *A&A*, 476, L13
 Barnes, J. W. 2007, *PASP*, 119, 986
 Batalha, N. M., Rowe, J. F., Bryson, S. T., et al. 2013, *ApJS*, 204, 24
 Bean, J. L., Seifahrt, A., Hartman, H., et al. 2010, *ApJ*, 713, 410
 Beatty, T. G., & Seager, S. 2010, *ApJ*, 712, 1433
 Bonfils, X., Gillon, M., Udry, S., et al. 2012, *A&A*, 546, A27
 Borucki, W. J., & Summers, A. L. 1984, *Icarus*, 58, 121
 Bouchy, F., Udry, S., Mayor, M., et al. 2005, *A&A*, 444, L15
 Burke, C. J. 2008, *ApJ*, 679, 1566
 Burke, C. J., Bryson, S., Christiansen, J., et al. 2013, in *American Astronomical Society Meeting Abstracts*, Vol. 221, American Astronomical Society Meeting Abstracts, #216.02
 Butler, R. P., Vogt, S. S., Marcy, G. W., et al. 2004, *ApJ*, 617, 580
 Butler, R. P., Wright, J. T., Marcy, G. W., et al. 2006, *ApJ*, 646, 505
 Chabrier, G., Baraffe, I., Allard, F., & Hauschildt, P. 2000, *ApJ*, 542, 464
 Charbonneau, D., Brown, T. M., Latham, D. W., & Mayor, M. 2000, *ApJ*, 529, L45
 Collier Cameron, A., Bouchy, F., Hébrard, G., et al. 2007, *MNRAS*, 375, 951
 Demory, B.-O., Gillon, M., Deming, D., et al. 2011, *A&A*, 533, A114
 Dumusque, X., Pepe, F., Lovis, C., et al. 2012, *Nature*, 491, 207
 Eisenstein, D. J., Weinberg, D. H., Agol, E., et al. 2011, *AJ*, 142, 72

- Feldt, M., Gratton, R., Hippler, S., et al. 2007, *The CHEOPS Project: Characterizing Exoplanets by Opto-infrared Polarimetry and Spectroscopy*, ed. A. P. Lobanov, J. A. Zensus, C. Cesarsky, & P. J. Diamond (Springer-Verlag), 261
- Fischer, D. A., Vogt, S. S., Marcy, G. W., et al. 2007, *ApJ*, 669, 1336
- Fleming, S. W., Ge, J., Barnes, R., et al. 2012, *AJ*, 144, 72
- Fossey, S. J., Waldmann, I. P., & Kipping, D. M. 2009, *MNRAS*, 396, L16
- Fressin, F., Guillot, T., Morello, V., & Pont, F. 2007, *A&A*, 475, 729
- Gaudi, B. S. 2005, *ApJ*, 628, L73
- Gaudi, B. S., Seager, S., & Mallen-Ornelas, G. 2005, *ApJ*, 623, 472
- Ge, J., Mahadevan, S., Lee, B., et al. 2008, in *Astronomical Society of the Pacific Conference Series*, Vol. 398, *Extreme Solar Systems*, ed. D. Fischer, F. A. Rasio, S. E. Thorsett, & A. Wolszczan, 449
- Gillon, M., Pont, F., Demory, B.-O., et al. 2007, *A&A*, 472, L13
- Grether, D., & Lineweaver, C. H. 2006, *ApJ*, 640, 1051
- Henry, G. W., Marcy, G. W., Butler, R. P., & Vogt, S. S. 2000, *ApJ*, 529, L41
- Ho, S., & Turner, E. L. 2011, *The Astrophysical Journal*, 739, 26
- Howard, A. W., Marcy, G. W., Johnson, J. A., et al. 2010, *Science*, 330, 653
- Ida, S., & Lin, D. N. C. 2004, *ApJ*, 604, 388
- . 2008, *ApJ*, 685, 584
- Kane, S. R., Ciardi, D., Fischer, D., et al. 2010a, in *Bulletin of the American Astronomical Society*, Vol. 42, *American Astronomical Society Meeting Abstracts #215, #328.02*
- Kane, S. R., Reffert, S., Henry, G. W., et al. 2010b, *ApJ*, 720, 1644
- Kane, S. R., & von Braun, K. 2008, *ApJ*, 689, 492
- . 2009, *PASP*, 121, 1096
- Kipping, D. M. 2008, *MNRAS*, 389, 1383
- Konacki, M., Torres, G., Jha, S., & Sasselov, D. D. 2003, *Nature*, 421, 507
- Lopez, S., & Jenkins, J. S. 2012, *ApJ*, 756, 177
- Lovis, C., Mayor, M., Pepe, F., et al. 2006, *Nature*, 441, 305
- Mahadevan, S., Ramsey, L., Bender, C., et al. 2012, in *Society of Photo-Optical Instrumentation Engineers (SPIE) Conference Series*, Vol. 8446, *Society of Photo-Optical Instrumentation Engineers (SPIE) Conference Series*
- Marcy, G. W., & Butler, R. P. 2000, *PASP*, 112, 137
- Mayor, M., Bonfils, X., Forveille, T., et al. 2009, *A&A*, 507, 487
- Mayor, M., Marmier, M., Lovis, C., et al. 2011, *ArXiv e-prints*
- McArthur, B. E., Endl, M., Cochran, W. D., et al. 2004, *ApJ*, 614, L81
- McCullough, P. R., Stys, J. E., Valenti, J. A., et al. 2006, *ApJ*, 648, 1228
- Mordasini, C., Alibert, Y., Benz, W., & Naef, D. 2009, *A&A*, 501, 1161
- Mordasini, C., Alibert, Y., Georgy, C., et al. 2012, *A&A*, 547, A112
- Moutou, C., Hébrard, G., Bouchy, F., et al. 2009, *A&A*, 498, L5
- Naef, D., Latham, D. W., Mayor, M., et al. 2001, *A&A*, 375, L27
- Plavchan, P., Anglada-Escud?, G., White, R. J., et al. 2013, in *American Astronomical Society Meeting Abstracts*, Vol. 221, *American Astronomical Society Meeting Abstracts*, #109.06
- Pont, F., Bouchy, F., Melo, C., et al. 2005, *A&A*, 438, 1123
- Raghavan, D., McAlister, H. A., Henry, T. J., et al. 2010, *ApJS*, 190, 1
- Rayner, J., & PRVS Team. 2007, in *Bulletin of the American Astronomical Society*, Vol. 39, *American Astronomical Society Meeting Abstracts #210, #110.02*
- Rivera, E. J., Butler, R. P., Vogt, S. S., et al. 2010, *ApJ*, 708, 1492
- Rivera, E. J., Lissauer, J. J., Butler, R. P., et al. 2005, *ApJ*, 634, 625
- Sackett, P. D. 1999, in *NATO ASIC Proc. 532: Planets Outside the Solar System: Theory and Observations*, ed. J.-M. Mariotti & D. Alloin, 189
- Sato, B., Fischer, D. A., Henry, G. W., et al. 2005, *ApJ*, 633, 465
- Seager, S. 2011, *Exoplanets* (The University of Arizona Press)
- Seagrove, S., Harker, J., Laughlin, G., Lacy, J., & Castellano, T. 2003, *PASP*, 115, 1355
- Siverd, R. J., Beatty, T. G., Pepper, J., et al. 2012, *ApJ*, 761, 123
- Spiegel, D. S., Burrows, A., & Milsom, J. A. 2011, *ApJ*, 727, 57
- Udalski, A., Paczynski, B., Zebrun, K., et al. 2002, *Acta Astronomica*, 52, 1
- Udry, S., Bonfils, X., Delfosse, X., et al. 2007, *A&A*, 469, L43
- von Braun, K., Kane, S. R., Mahadevan, S., et al. 2011, in *European Physical Journal Web of Conferences*, Vol. 11, *European Physical Journal Web of Conferences*, 6006
- Watson, C. A., Littlefair, S. P., Collier Cameron, A., Dhillon, V. S., & Simpson, E. K. 2010, *MNRAS*, 408, 1606
- Weiss, L. M., Marcy, G. W., Rowe, J. F., et al. 2013, *ApJ*, 768, 14
- Weldrake, D. T. F., Bayliss, D. D. R., Sackett, P. D., et al. 2008, *ApJ*, 675, L37
- Winn, J. N. 2011, *Exoplanet Transits and Occultations*, ed. S. Seager (The University of Arizona Press), 55–77
- Winn, J. N., Matthews, J. M., Dawson, R. I., et al. 2011a, *ApJ*, 737, L18
- . 2011b, *ApJ*, 737, L18
- Wisniewski, J. P., Ge, J., Crepp, J. R., et al. 2012, *AJ*, 143, 107
- Wright, J. T., Fakhouri, O., Marcy, G. W., et al. 2011, *PASP*, 123, 412